







Recent speciation and hybridization in Icelandic deep-sea isopods: An integrative approach using genomics and proteomics

Eva Paulus^{1,2}  | Saskia Brix²  | Annabelle Siebert^{2,3} | Pedro Martínez Arbizu⁴  |
Sven Rossel⁴  | Janna Peters⁴ | Jörundur Svavarsson⁵  | Martin Schwentner^{3,6} 

¹University of Groningen, Groningen, The Netherlands

²Senckenberg am Meer, German Centre for Marine Biodiversity Research (DZMB), Hamburg, Germany

³Center of Natural History (CeNak), Universität Hamburg, Hamburg, Germany

⁴Senckenberg am Meer, German Centre for Marine Biodiversity Research (DZMB), Wilhelmshaven, Germany

⁵Department of Life and Environmental Sciences, University of Iceland, Reykjavik, Iceland

⁶Naturhistorisches Museum Wien, Vienna, Austria

Correspondence

Saskia Brix, Senckenberg am Meer, German Centre for Marine Biodiversity Research (DZMB) c/o Biocenter Grindel, Center of Natural History (CeNak), Universität Hamburg, Hamburg, Germany. Email: saskia.brix-elsig@senckenberg.de

Funding information

Deutsche Forschungsgemeinschaft, Grant/Award Number: BR3843/4-1, BR3843/5-1, RE2808/3-1 and RE2808/3-2

Abstract

The crustacean marine isopod species *Haploniscus bicuspis* (Sars, 1877) shows circum-Icelandic distribution in a wide range of environmental conditions and along well-known geographic barriers, such as the Greenland-Iceland-Faroe (GIF) Ridge. We wanted to explore population genetics, phylogeography and cryptic speciation as well as investigate whether previously described, but unaccepted subspecies have any merit. Using the same set of specimens, we combined mitochondrial COI sequences, thousands of nuclear loci (ddRAD), and proteomic profiles, plus selected morphological characters using confocal laser scanning microscopy (CLSM). Five divergent genetic lineages were identified by COI and ddRAD, two south and three north of the GIF Ridge. Assignment of populations to the three northern lineages varied and detailed analyses revealed hybridization and gene flow between them, suggesting a single northern species with a complex phylogeographic history. No apparent hybridization was observed among lineages south of the GIF Ridge, inferring the existence of two more species. Differences in proteomic profiles between the three putative species were minimal, implying an ongoing or recent speciation process. Population differentiation was high, even among closely associated populations, and higher in mitochondrial COI than nuclear ddRAD loci. Gene flow is apparently male-biased, leading to hybrid zones and instances of complete exchange of the local nuclear genome through immigrating males. This study did not confirm the existence of subspecies defined by male characters, which probably instead refer to different male developmental stages.

KEYWORDS

cryptic species, ddRAD, DNA barcoding, Haploniscidae, *Haploniscus bicuspis*, MALDI-TOF

This is an open access article under the terms of the Creative Commons Attribution-NonCommercial License, which permits use, distribution and reproduction in any medium, provided the original work is properly cited and is not used for commercial purposes.

© 2021 The Authors. *Molecular Ecology* published by John Wiley & Sons Ltd.

1 | INTRODUCTION

Deep-sea benthos fosters a high diversity of invertebrates with peracarid crustaceans like Isopoda being particularly species-rich (Brandt et al., 2018; Brandt et al., 2012; Wilson & Ahnyong, 2015). The underlying factors that shaped this diversity and the potential role of past climatic changes or physical barriers, such as deep-sea ridges, are not well understood. Similarly, fundamental population genetic studies are scarce for the deep sea and most utilize one or a few markers (reviewed in Taylor & Roterman, 2017). Studies on deep-sea peracarids using modern genomic population genetic techniques like RAD-sequencing are still rare (e.g., Schwentner & Lörz, 2021; Timm et al., 2018). One problem is the limited availability of large-scale data sets in terms of individual numbers and geographic scale. The deep-sea crustacean isopod species *Haploniscus bicuspis* (Sars, 1877) is an ideal model to study diversity in this environment, as it is one of the few isopod species with circum-Icelandic distribution and there are large numbers of samples available from the Benthic Invertebrates of Icelandic Waters (BIOICE) and Icelandic marine Animals: Genetics and Ecology (IceAGE) projects (Brix et al., 2014; Meißner et al., 2018).

The complex interactions of highly diverse water masses make Icelandic waters an interesting location to study the distribution and speciation processes of deep-sea taxa. While the water is warmer and more saline in the North Atlantic south of Iceland, the colder waters of the Nordic Seas and the Arctic Ocean shape the environment to the North. Steep gradients in temperature and salinity, various sediment substrates, differences in food availability, and several shallow and deep ridges create a unique and diverse environment. This favours high biodiversity through a patchwork of different habitats within relatively small scales (Brökeland & Svavarsson, 2017; Jochumsen et al., 2016; Meißner et al., 2014; Ostmann et al., 2014).

For other isopod (Brix & Svavarsson, 2010) and amphipod (Dauvin et al., 2012; Weissshappel, 2000, 2001) crustaceans, as well as many other benthic deep-sea animals, the Greenland-Iceland-Faeroe (GIF) Ridge is an important barrier that limits their distribution. The GIF Ridge has a saddle depth of about 480 m between the Faeroe Islands and Iceland in the southeast, and 620 m between Greenland and Iceland in the northwest of Iceland (Hansen & Østerhus, 2000). Near-bottom temperatures range from 12°C in the North Atlantic south of the GIF Ridge, to -0.9°C deep north of the GIF Ridge (Jochumsen et al., 2016; Schnurr et al., 2014). Iceland is located in an area especially susceptible to climatic change (Hanna et al., 2006) and hence is undergoing rapid changes in terms of species distribution and composition (e.g., Arnason, 2007; D'Alba et al., 2010; Pecl et al., 2017). Naturally, the waters around Iceland have been influenced by past climatic changes. During the Last Glacial Maximum, the ice sheet extended beyond the Icelandic landmass and within reach of the shelf break at around 300 m depth (Patton et al., 2017). Around 15 ka BP, the ice sheet broke apart abruptly due to rising sea levels (Geirsdóttir et al., 2009; Norðdahl & Ingólfsson, 2015). Both the southern (i.e., Iceland-Faeroe Ridge) and the northern parts of the GIF Ridge (i.e. Denmark Strait between Iceland and Greenland)

were probably influenced by spreading and contracting ice sheets, potentially limiting the distribution of benthic marine animals.

The GIF Ridge and associated ecological differences strongly affect the observed species compositions with most benthic deep-sea species (e.g., Isopoda, Amphipoda, Tanaidacea) being confined to one side of the GIF Ridge (e.g., Brix, Lörz, et al., 2018; Brix, Stransky, et al., 2018; Gudmundsson, 1998; Hansen, 1908; Jakiel et al., 2018; Negoescu & Svavarsson, 1997; Stransky & Svavarsson, 2006; Svavarsson et al., 1993; Weissshappel, 2001).

An interesting exception is the widespread asellote isopod species *Haploniscus bicuspis* (Figure 1). It occurs in all water masses and in various sampled depths (300–2900 m) around Iceland, whereas the majority of congeneric species are confined to the North Atlantic Ocean (except for *H. angustus* Lincoln, 1985; Brökeland & Svavarsson, 2017). This makes *H. bicuspis* an ideal model to study patterns of genetic diversity, population genetics and the phylogeographic history of a benthic deep-sea isopod species. It also offers the possibility to assess proteomic differences using matrix-assisted laser desorption/ionization time-of-flight mass spectrometry (MALDI-TOF MS) associated with ecological differentiation or potential cryptic speciation. Species identification with MALDI-TOF MS is well-established in microbiology for determination of bacteria, viruses, and fungi (Nachtigall et al., 2020; Singhal et al., 2015) and several proof-of-concept studies supported its general applicability for species delimitation in marine crustaceans (Riccardi et al., 2012; Laakmann et al., 2013; Bode et al., 2017; Rossel and Martínez Arbizu, 2018), yet to our knowledge no studies on peracarids have been performed so far. Understanding the taxonomic resolution of proteomic profiling in invertebrates is the subject of ongoing research.

Haploniscus bicuspis was first described from specimens collected near Norway (Figure S1, Sars, 1877). Subsequently, Wolff (1962) described two subspecies based on the shape of the male antennula and pleopod 1 (see Figure 2): *Haploniscus bicuspis bicuspis* (including the Norwegian specimens) and *H. bicuspis tepidus* (from the Reykjanes Ridge southwest of Iceland). The latter features a narrower second segment of the antennula and a laterally rounded distal part of the pleopod 1 (in contrast to the presence of a distinct corner in *H. b. bicuspis*; Figure 2). Unfortunately, the type series of *H. bicuspis* comprises no adult male and both subspecies of Wolff (1962) currently hold the status “unaccepted” in WoRMS (Boyko et al., 2008., accessed August 2020). It is currently unknown whether the morphological variation described by Wolff suggests cryptic speciation or intraspecific variability.

Asellote isopods are particularly interesting for population genetic studies, as a pelagic larval stage is absent in their life cycle. Like all Peracarida, they hatch and rear juveniles in a brooding pouch (marsupium), and the juveniles largely resemble the adult morphology and lifestyle upon release (Lincoln, 1985). This limits their dispersal abilities compared to animals with free-swimming pelagic life stages. In general, locomotion and dispersal abilities in deep-sea asellote isopods depend on the adult stage (Brix et al., 2020). In the abyssal Pacific, Haploniscidae showed a mean species range of 183 km and a maximum range of 1310 km, with 83%

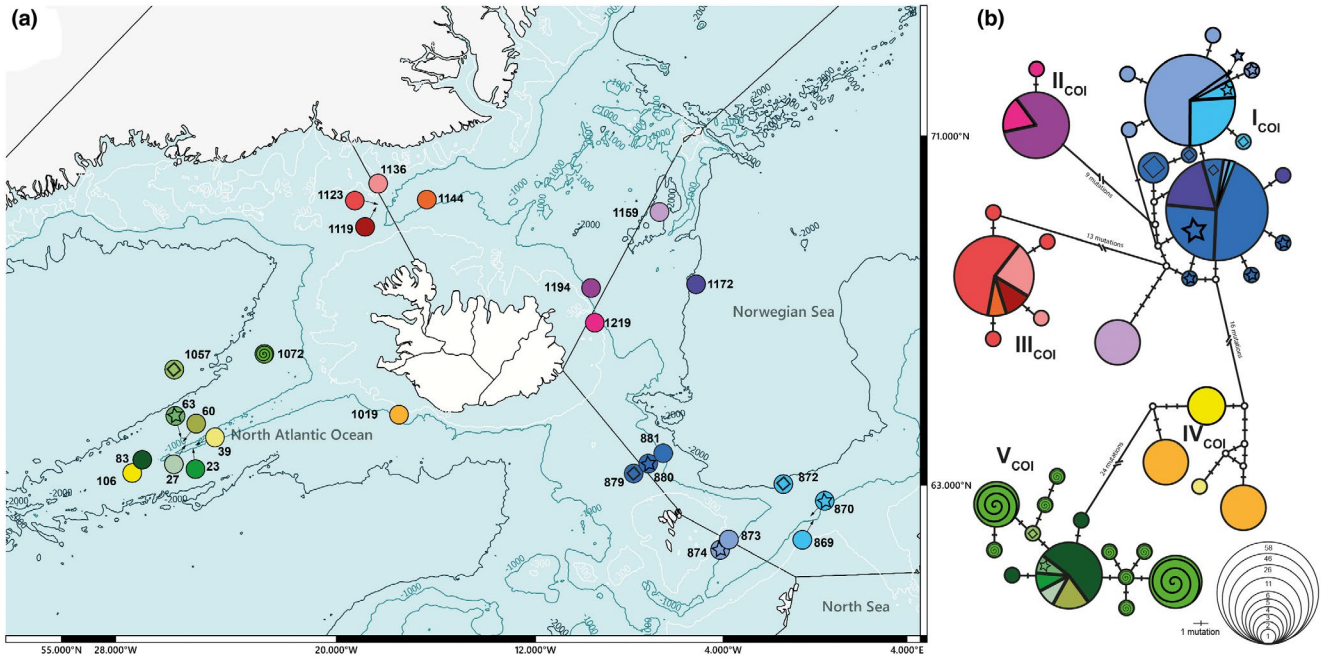


FIGURE 1 (a) Distribution map of *Haploniscus bicuspis* sampled in this study collected during three IceAGE expeditions. Numbers refer to station numbers. (b) COI haplotype network calculated with Network. Colours correspond to stations

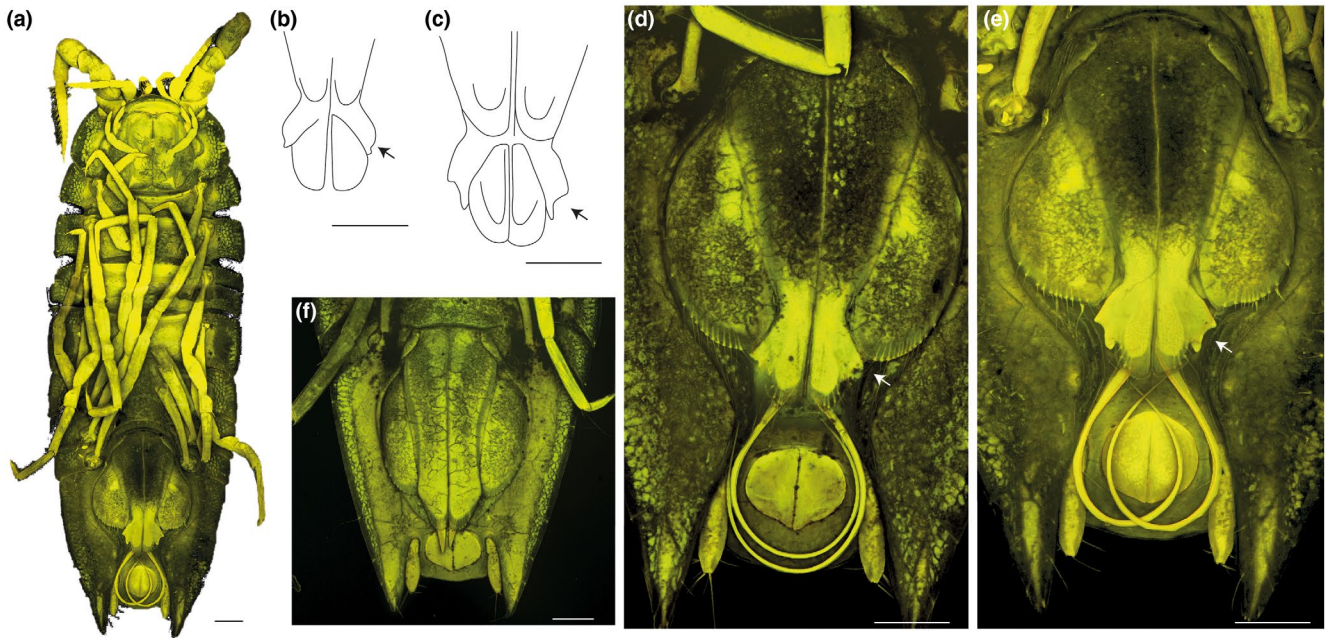


FIGURE 2 Morphology of male pleopod 1 for (sub)species delimitation. (a) ventral view of complete adult male (ZMH-K 60856, lineage I; head facing upwards), (b) male pleopod 1 of *H. bicuspis tepidus*, (c) male pleopod 1 of *H. bicuspis bicuspis*, (d) and (e) pleopod 1 of adult males (ZMH-K 60196 and ZMH-K 60856, both lineage I) and (f) pleopod 1 of juvenile male (ZMH-K 60066, lineage I). (c) and (d) redrawn after Wolff (1962). Arrows indicate the distal part of pleopod 1, which is supposed to show species-specific differences (laterally rounded in *H. b. tepidus*, distinct corner in *H. b. bicuspis*). (a), (d), (e) and (f) were taken with a CLSM. Scale bar = 100 μ m

of the species ($n = 24$) present in a single area only (Brix et al., 2020). These distributional ranges are much lower than for the swimming isopod families Desmosomatidae and Munnopsidae. As

a typical walking haploniscid isopod, the body plan of *Haploniscus* does not show adaptations specific to swimming or burrowing, and the animals are found in close association with the sediment

surface (Brix et al., 2020; Thiel & Haye, 2006). This suggests comparably poor dispersal capabilities of the adults as well.

This study aimed to explore the genetic diversity within *Haploniscus bicuspis*, focusing on aspects of potential cryptic diversity, population genetics and its phylogeographic history. The latter is particularly interesting as it may reveal historic glacial refugia and postglacial (re-)colonization for a deep-sea species, and thus potential population genetic consequences of past climatic changes. To do so, we combined analyses of mitochondrial COI sequences with up to 2993 nuclear ddRAD loci. We further assessed proteome-level differences between populations and putatively revealed cryptic species.

2 | MATERIALS AND METHODS

2.1 | Sampling design

All *H. bicuspis* specimens examined were sampled aboard the research vessels RV Meteor (M85/3), RV Poseidon (POS456) and RV Maria S. Merian (MSM75) during the IceAGE (2011), IceAGE2 (2013) and IceAGE_RR (2018) expeditions. The specimens were sorted at the laboratories of the DZMB (German Centre for Marine Biodiversity Research) and deposited in the collections of the Centre of Natural History in Hamburg (Table S1). Specimens were collected using an epibenthic sledge (EBS, see Brenke, 2005), except for samples from stations 23 and 63, which were collected using a Van Veen grab.

2.2 | Taxonomic and morphological analyses

The following type material from the Museum in Copenhagen was morphologically compared to the newly collected IceAGE specimens:

A dry vial apparently containing 1 dried specimen and labelled as ZMUC-CRU-5817 from Ingolf st. 78; The slide portion of ZMUC-CRU-5817; a dry vial containing 2 microvials of *H. b. bicuspis* from Ingolf st. 112; a dry vial containing 1 microvial of *H. b. bicuspis* from Ingolf st. 139; a vial with about 20 specimens in alcohol labelled as ZMUC-CRU-346, but also with the following label from Institut für Polarökologie, Kiel (not Zoological Museum): *Haploniscus bicuspis*, Projekt H21-5, Station 333, Gerät EBS, Sammler A. Brandt.; the nonslide portion of ZMUC-CRU-5817 (NHMD-83661) consists of 1 syntype of *H. b. tepidus* in alcohol; the two dried syntypes of this subspecies from Ingolf st. 78 labelled as NHMD-272194; a dry vial containing 1 microvial of *H. b. bicuspis* from Ingolf st. 104; a dry vial containing 1 microvial of *H. b. bicuspis* from Ingolf st. 125; ZMUC-CRU-346 (NHMD-78194) with ZMUC supplementary label (Meteor st. 333, Kolbeinsey Ridge, Iceland, 67°56.5'N, 18°02.4'W).

Selected males were visualized using confocal laser scanning microscopy (CLSM), an optical imaging technique, to assess pleopod 1 morphology. Specimens were stained with the fluorescent markers Congo Red and Acid Fuchsin (1:1) following the methodology

outlined in Michels and Büntzow (2010). For scanning, specimens were transferred to glycerin. A Leica TCS SPV with a Leica DM5000 B microscope and DPSS laser (10 mW, 561 nm) was used to perform the CLSM. Scans were recorded with the LAS AF 2.2. software.

2.3 | Molecular analyses

DNA extractions were performed using the mid-sections of the animals, leaving the cephalothorax and the pleon intact for subsequent morphological analyses and as partial vouchers in the collections. The animals were dissected carefully using a micro scissor and the gut was removed to avoid contaminations. If possible, the same animal was used for proteomics, COI barcoding and ddRAD, transferring half of the dissected tissue in a vial for genetics and the other half into a vial for proteomics. DNA was extracted using the marine animal tissue genomic DNA extraction kit (Neo Biotech) or the Genomic DNA from tissue kit (Macherey-Nagel). DNA was eluted in 70 µl elution buffer. Chelex (Chelating ion exchange resin, Bio-Rad) was used for some of the animals for which only the COI fragment was sequenced (for protocol see Jennings et al., 2020).

2.3.1 | COI

Using 1 µl DNA extract, the DNA was PCR amplified using PuReTaq Ready-To-Go (RTG) PCR Beads (GE Healthcare) with 1 µl of either dgLCO (GGT CAA CAA ATC ATA AAG AYA TYG G; Meyer, 2003)/ dgHCO (TAA ACT TCA GGG TGA CCA AAR AAY CA; Meyer, 2003) or LCOJJ (CHACWAAAYCATAAAGATATYGG; Astrin & Stüben, 2008)/ HCOJJ (AWACTTCVGGRTGVCCAAARAATCA; Astrin & Stüben, 2008) primers and 22 µl nuclease-free water. The PCR ran at 94°C for 5 min, followed by 38 cycles of denaturation at 94°C for 45 s, annealing at 45°C for 50 s, and elongation at 72°C for 1 min. This was followed by the final elongation at 72°C for 5 min. The resulting fragment length was assessed by gel electrophoresis using 1.5% TAE gels. Excess primers were removed using ExoSAP. The PCR products and the corresponding primers were sent to Macrogen or Eurofins for bidirectional DNA Sanger sequencing.

The resulting sequences were individually checked for their quality using GENEIOUS Prime version 2019.2.3 and the forward and reverse sequences were assembled using the *de novo* assembly function. An alignment was created using MUSCLE version 3.8.425 (Edgar, 2004). To assess the potential presence of cryptic diversity within *H. bicuspis*, we employed three species delimitation methods: generalized mixed Yule coalescent model (GMYC; Pons et al., 2006), automatic barcode gap discovery (ABGD; Puillandre et al., 2012) and assemble species by automated partitioning (ASAP; Puillandre et al., 2012). GMYC is an R script, it was run with the single, as well as with the multiple threshold method (Reid & Carstens, 2012). The GMYC method uses an ultrametric tree as input to delimit clusters of putative species. The ultrametric tree was generated with BEAST2 (Bouckaert et al., 2019), running the analyses for 30 million

generations, employing the Yule model and including every observed COI haplotype once. ABGD uses the so-called barcode gap, which corresponds to the gap between intra- and interspecific genetic distances, to delimit putative species. We used the web version of ABGD (see <https://bioinfo.mnhn.fr/abi/public/abgd/abgdweb.html>) with standard settings except for a relative gap width of 0.5 and 100 steps and the uncorrected p -distances, precalculated with MEGA-X version 10.0.5 (Kumar et al., 2018). ASAP also delimits putative species based on genetic distance distributions. We used the web version (<https://bioinfo.mnhn.fr/abi/public/asap/asapweb.html>) with standard settings. An unrooted phylogenetic network was calculated with SplitsTree (Huson & Bryant, 2006) to visualize the divergence between putative species (henceforth called lineages).

To assess the distribution of genetic diversity and the phylogeographic history, a median-joining haplotype network was generated using the program Network v 10.0 (see fluxus-engineering.com; Bandelt et al., 1999) and redrawn using INKSCAPE (<http://www.inkscape.org>). Furthermore, for each population (i.e., sampling station) nucleotide diversity (π) and gene diversity (h) were calculated with Arlequin 3.5.2.2 (Excoffier & Lischer, 2010). The demographic parameters Tajima's D and Fu's F , which assess deviations from neutrality (e.g., differentiating evolutionary random from nonrandom processes such as selection, population expansion or contraction), were also assessed. Genetic differentiation between populations was evaluated using pairwise F_{ST} , calculated only among populations of the same lineage and among the very closely associated lineages I_{COI}-III_{COI} (see below). These F_{ST} values were also used to assess isolation-by-distance via a Mantel test in Arlequin in which the F_{ST} values and geographic distance in km were tested for correlation. For Tajima's D , Fu's F , and F_{ST} only populations with at least five individuals available were included.

2.3.2 | ddRAD

Based on DNA yield, a subset of samples was selected for ddRAD sequencing. Usually selected samples had >150 ng DNA. To include certain relevant populations, a few samples with >30 ng DNA were selected as well. DNA concentration was measured with a Qubit 3.0 (Invitrogen). If samples had less than 150 ng DNA, they were concentrated via drying. All samples were brought to 24 μ l. The protocol described by Peterson et al. (2012) was mostly adhered to, with a few modifications (see also Franchini et al., 2017; Schwentner & Lörz, 2021). Samples were grouped in batches of eight based on DNA concentration. Restriction digestion was carried out at 37°C for 4 h using 3 μ l fastdigest buffer, 1.5 μ l fastdigest MspI and fastdigest EcoRI enzymes each (Thermo Fisher Scientific), following Schwentner and Lörz (2021). Digested DNA was cleaned using 1.5 \times volume of magnetic beads and eluted in 21 μ l H₂O (AmpliClean Cleanup Kit, Nimagen). MspI and EcoRI adapters were ligated to the 19 μ l digested DNA using 3 μ l of each adaptor (EcoRI adaptor 2 μ M, MspI adaptor 31.6 μ M), 3 μ l of 10 \times T4 ligase buffer, and 2 μ l T4 ligase (1–2 Weiss units). 16 EcoRI and 8 MspI adapter variations with

unique barcodes (MspI adapters with four additional random nucleotides, as described in Franchini et al., 2017) were used to provide a unique barcode combination for each sample within each batch of eight samples (Table S1). Ligation commenced at 22°C for 1 h and was heat-terminated at 65°C for 10 min. Afterwards, the eight samples of each batch were pooled, and the pools were cleaned up using 1.5 \times volume of magnetic beads, eluting in 30 μ l of TE buffer. DNA fragments of 300 base pairs (bp) were selected with a BluePippin (Sage Science, \pm 30 bp allowed, "tight" setting) using a 1.5% agarose gel cassette with DF marker R2.

To reduce PCR amplification biases, four PCR replicates were run for each pool after size selection. PCRs comprised 5 μ l 2 \times Kappa HS HIFI mix, 0.3 μ l of each primer and 4.4 μ l library. Forward and reverse primers included eight different 8 bp indices (Table S1) and were combined to add a unique index combination for each pool. The two-step PCR program ran at 95°C for 3 min, followed by 15–19 cycles (depending on initial DNA concentration) of 98°C for 20 s, 72°C for 25 s, and final elongation at 72°C for 1 min. The four replicates of each library were combined and cleaned up using 1 \times volume of magnetic beads, eluting in 18 μ l H₂O. DNA concentration was measured using a Qubit and mean size assessed using a TapeStation (Agilent). All samples were pooled at equal molarity and sent off to MacroGen for sequencing on one Illumina HiSeq4000 lane (100 bp, paired-end).

The reads were predemultiplexed by indices by MacroGen upon delivery. Potential PCR duplicates were removed using the clone_filter function of STACKS (Rochette et al., 2019) and the demultiplexing by barcodes was performed with the process_radtags function. Assembly of loci was performed using ipyrad (Eaton & Overcast, 2020). Parameters were optimized in multiple test runs and specimens with less than 50% of retrieved loci were removed after initial test runs. The crucial parameters in the final analyses were set to: no. 14 (clust_threshold) = 0.91, no. 20 (max_Hs_consens) = 0.1, and no. 22 (max_SNPs_locus) = 0.15 (see File S1 for full set of parameters). To further optimize the number of retrieved loci, two different runs were performed: one including all specimens and one including all specimens previously delimited into lineages I_{COI}-III_{COI}. The latter run was performed to optimize loci recovery for this set of genetically and geographically closely associated lineages. In all analyses, a "populations" file was included (defining lineages retrieved by COI) and requiring at least 50% of specimens of each population to be represented for a locus to be retained. The number of putatively non-neutrally evolving loci was determined with BayeScan (Foll & Gaggiotti, 2008) for each data set. With less than 1.5% of loci being identified as putatively non-neutral, the overall data sets are well-suited for further analyses.

To assess if the nuclear ddRAD data support the lineages differentiated by COI phylogenetic networks, principal component analyses (PCA), Structure and coancestry analyses were performed on each of the three ddRAD data sets. Unrooted phylogenetic networks were computed with SplitsTree. PCA and Structure analyses were run via Python scripts provided on the ipyrad homepage (<https://ipyrad.readthedocs.io/en/latest/API-analysis/index.html>;

visited 10 March, 2020) using the.snps.hdf5 ipyrad output files. A minimum coverage of 80% was set for each locus. For PCA, all available SNPs were included, but for Structure only one SNP of each locus was included to reduce artefacts by linkage. Structure analyses ran for 500,000 generations, with a burnin of 50,000 generations, for $k = 2$ to $k = 8$ and with five replicates each. In each replicate, one SNP was randomly selected per locus. The replicates were summarized with CLUMPP (Jakobsson & Rosenberg, 2007). The best-fitting k was identified based on ad hoc posterior probability models of [Pr(X|K)] (Pritchard et al., 2000) and deltaK (Evanno et al., 2005) using the web version of STRUCTURE HARVESTER (see <http://taylor0.biology.ucla.edu/structureHarvester/>, accessed 23 July, 2020; Earl & vonHoldt, 2012). The output of the best-fitting k was plotted with the online version of StructurePlot v2 (<http://omics.speaks.com/strplot2/>; Ramasamy et al., 2014) sorting individuals by similarity. Coancestry analyses used RADpainter and fineRADstructure (Malinsky et al., 2018) closely following the proposed usage (<https://cichlid.gurdon.cam.ac.uk/fineRADstructure.html>, accessed 1 December, 2020). The results were plotted using the provided R script FinestructureLibrary.R (<https://github.com/millanek/fineRADstructure/blob/master/FinestructureLibrary.R>, accessed 1 December, 2020). One great advantage of the coancestry analysis compared to Structure is the utilization of the complete nuclear haplotypes instead of a single SNP per locus. The vcf files from ipyrad were used as input.

Key population genetic and demographic parameters were calculated from the vcf files generated by ipyrad. Nucleotide diversity, Tajima's D , the inbreeding coefficient F_{IS} and pairwise F_{ST} values were calculated for each locus with VCFtools (Danecek et al., 2011) and then averaged for each lineage and population. Nucleotide diversities were corrected by the total number of nucleotides. Heterozygosity per site per individual was reported by ipyrad and summarized (as a mean value) for each lineage and population. Isolation-by-distance was assessed with a Mantel test in Arlequin as described above for COI. We further tested for a correlation between population differentiation (F_{ST}) based on COI and based on ddRAD loci by performing a Mantel test in Arlequin. To assess demographic changes over time, extended Bayesian skyline plots (EBSP; Figure S4) were calculated with BEAST2 for lineages I–III jointly, as these probably constitute a single species with interlineage hybridization (see discussion). Three runs were performed, one using the COI data set, and two runs each using 200 randomly chosen ddRAD loci (nonoverlapping among runs), selecting only loci with 5–10 SNPs each. Loci were retrieved from the *snpsmap ipyrad outputfile. Among loci, the site and clock models were linked, but the tree models unlinked. The HKY model was selected with four gamma categories, empirical frequencies and kappa 2.0. A strict clock with a rate of 1 was enforced, as no suitable substitution rates are available (a few crustacean COI substitution rates have been published, their applicability to deep-sea Isopoda is questionable; see also Loeza-Quintana et al., 2019). The coalescent extended Bayesian skyline prior was selected for each locus. The weights for indicatorSampler.alltrees and indicatorScaler.alltrees were set to 5000, of EBSPupDownOperator.alltrees to 3000 and of

"bitflip.alltrees" to 10,000. The MCMC chain was run for 100×10^6 generations, sampling every 5000th for EBSP. The output was analysed with the EBSPAnalyser included in the BEAST2 package, discarding the first 25% as burnin. The final data including the 95% highest probability density intervals was plotted in R (R Core Team, 2020).

2.4 | Matrix-assisted laser desorption/ionization time-of-flight mass spectrometry

In MALDI-TOF MS analyses, peptides and proteins are extracted and embedded in a matrix solution enabling mass-detection of large molecules. Because numerous proteins are measured simultaneously, analyses result in a proteome fingerprint that can be used to identify species. For measurements using MALDI-TOF MS, the same tissue was used from a subset of the genetically studied individuals, always including a single pereopod with the attached muscles. Tissue was incubated in 5 μ l of a matrix solution containing α -Cyano-4-hydroxycinnamic acid (HCCA) as a saturated solution in 50% acetonitrile, 47.5% molecular grade water and 2.5% trifluoroacetic acid. After 5 min of incubation, 1.5 μ l of the extract solution was applied to one spot for crystallization on a target plate. Measurements were carried out on a Microflex LT/SH System (Bruker Daltonics), employing the flexControl version 3.4 (Bruker Daltonics) software. Measured mass range was set from 2 k to 20 k Dalton. For peak evaluation, mass peak range from 2 k to 10 k Dalton was analysed using a centroid peak detection algorithm, a signal-to-noise threshold of 2, and a minimum intensity threshold of 600, with a peak resolution higher than 400. The proteins/pligonucleotide method was employed for fuzzy control with a maximal resolution ten times above the threshold. For a sum spectrum, 200 satisfactory shots were summed up. Three mass spectra were measured for each specimen. Quality control by eye was carried out and mass spectra of inferior quality were discarded. In the following analyses, only specimens with a respective COI sequence were used. For comparison of inter- and intraspecific variance spectra of the congener species, *H. foresti* ($n = 9$), *H. angustus* ($n = 4$) and *H. hamatus* ($n = 5$) were used (see Table S1).

Data processing was carried out in R (R Core Team, 2020) using packages MALDIquant (Gibb & Strimmer, 2012) and MALDIquantForeign (Gibb, 2015). Protein mass spectra were trimmed to an identical range from 2000 to 20,000 m/z and smoothed with the method employed by Savitzky and Golay (1964). The baseline was removed based on the SNIP baseline estimation method (Ryan et al., 1988) using 15 iterations. Mass spectra were normalized using the TIC method implemented in MALDIquant. Noise estimation was carried out with a signal to noise ratio (SNR) of 7. Repeated peak binning was carried out with a tolerance of 0.002 in a strict approach and resulting bins were aligned using R package MALDIrppa (Palarea-Albaladejo et al., 2018). For the resulting intensity matrix, missing values were interpolated from the corresponding spectrum. All signals below a SNR of 1.75 were assumed to be below detection limit and set to zero in the final peak matrix.

This matrix was Hellinger transformed (Legendre & Gallagher, 2001) for further use. Intra- and interspecific Euclidean distances were calculated using *vegdist* from R package *vegan* (Oksanen et al., 2013). To test group differentiation for classification approaches and to assess mass peak importance for group differentiation a Random Forest (RF, Breiman, 2001) analysis was carried out using R package *randomForest* (Liaw & Wiener, 2002, *ntree* = 2000, *mtry* = 35). Significant deviation from random of the observed model errors was calculated with the function *MVSF.test* from package *RFTools* (<https://github.com/pmartinezarbizu/RFTools>; Rossel & Martínez Arbizu, 2018). Significance of differences were tested using the distance-based multivariate analysis of variance (W_d^*) developed by Hamidi et al. (2019).

2.5 | Species distribution models

We modelled the distribution of the three main lineages retrieved by the genetic analyses (I–III, IV and V) based on major environmental factors. Random Forest classification models (Breiman, 2001) were calculated in R (R Core Team, 2020) using the package *randomForest* (Liaw & Wiener, 2002). The models were based on 2000 random trees and one third of all variables randomly sampled at each split (Liaw & Wiener, 2002).

Two types of models were calculated: (a) a multiclass model in which all three lineages (I–III, IV and V) are present and the model decides on the most probable class, and (b) a separate model for each lineage in which the model computes the probability of presence and absence for each lineage separately. For type (b), a presence/absence matrix was produced for the lineages I–III_{RAD}, IV_{RAD} and V_{RAD}. To avoid bias towards the absence class (which is most common), each tree was calculated with the same number of absence (randomly chosen) and presence. Predictor layers including the major environmental forces structuring the area (depth, bottom water salinity and temperature, bottom water oxygen, and particulate organic carbon flux [POC]) were downloaded from the global marine environmental data set (GMED; <http://gmed.auckland.ac.nz>). Probability of occurrence was predicted using the resulting models on a data set containing 88,822 geographic locations in the study area, after excluding locations situated on land or those lacking values in one or more predictor variables. Significant deviation from random of the observed model errors was calculated with the function *MVSF.test* from package *RFTools* (<https://github.com/pmartinezarbizu/RFTools>).

3 | RESULTS

3.1 | COI and ddRAD data sets

COI sequences of 211 *H. bicuspis* specimens were obtained. The final alignment was 530 bp long, of which 132 bp were parsimony-informative. Stop codons or indels were not observed. Only 52 of 78 sequenced ddRAD libraries were of sufficient quality for further

TABLE 1 Overview of ddRAD analyses

	All lineages	I _{RAD} –III _{RAD}
Number of loci	1723	2993
Total base pairs	290,828	502,577
Number of SNPs	18,999	21,697
Monomorphic base pairs	271,829 (93.47%)	480,880 (95.68%)
Monomorphic loci	9 (0.52%)	79 (2.64%)

Note: The ddRAD data was analysed once including all individuals and once including only individuals assigned to lineages I_{RAD}–III_{RAD}.

analyses. By discarding low-quality ddRAD libraries, a few relevant populations were not represented in the final ddRAD data sets. The two ddRAD data sets comprised 1723 and 2993 loci with 18,999 and 21,697 bp, respectively, and the vast majority of loci yielded one or more SNPs (Tables 1 & S2).

3.2 | Genetic diversity and species delimitation

The data from COI and ddRAD revealed deep genetic divergences within *H. bicuspis*. Because the assignment of individuals to lineage differed between COI and ddRAD, we will denote each lineage with a subscript index denoting the respective data type on which the lineage is based (we will omit these indices in the discussion, once lineages are treated as distinct species). In COI, *H. bicuspis* was split into several lineages (= putative species), with GMYC “single threshold” suggesting seven, GMYC “multiple threshold” six, ASAP five (*p*-value 6.87e-02; *W* value 6.17e-05; threshold distance 0.0128), and ABGD four lineages (for maximum intralocus uncorrected *p*-distance of 0.8%–2.1%). Based on the distance distribution and the Splitstree network (Figure 3c), we decided to work with the following five lineages: I_{COI} (east to southeast of Iceland; including station 1159 which was separated by GMYC “single threshold”), II_{COI} (east of Iceland, close to the shelf; I_{COI} and II_{COI} were combined in ABGD), III_{COI} (north of Iceland), IV_{COI} (south and southwest of Iceland; split into two syntopic lineages by GMYC single and multiple threshold), and V_{COI} (west and southwest of Iceland) (Figure S1, Table 2). None of these five lineages were syntopically recorded, and most lineages were clearly geographically separated. Only lineages IV_{COI} and V_{COI} occurred sympatrically along the Reykjanes Ridge. Lineage V_{COI} was genetically the most divergent lineage with uncorrected interlineage *p*-distances of 4.9%–7.3%.

In the nuclear ddRAD data, five lineages could also be delimited, with the two lineages south of the GIF Ridge corresponding to the COI data. However, the assignment of populations north of the GIF Ridge differed in some important aspects (Figure S2, Table 3). To better discern these lineages north of the GIF Ridge, separate ipyrad analyses were performed for lineages I–III, including PCA, Structure, and coancestry analyses. I_{RAD} includes only southeastern populations along the GIF Ridge towards the Faeroe Islands. Stations 1159 and 1172, which were also assigned to I_{COI}, clustered with the near-shelf

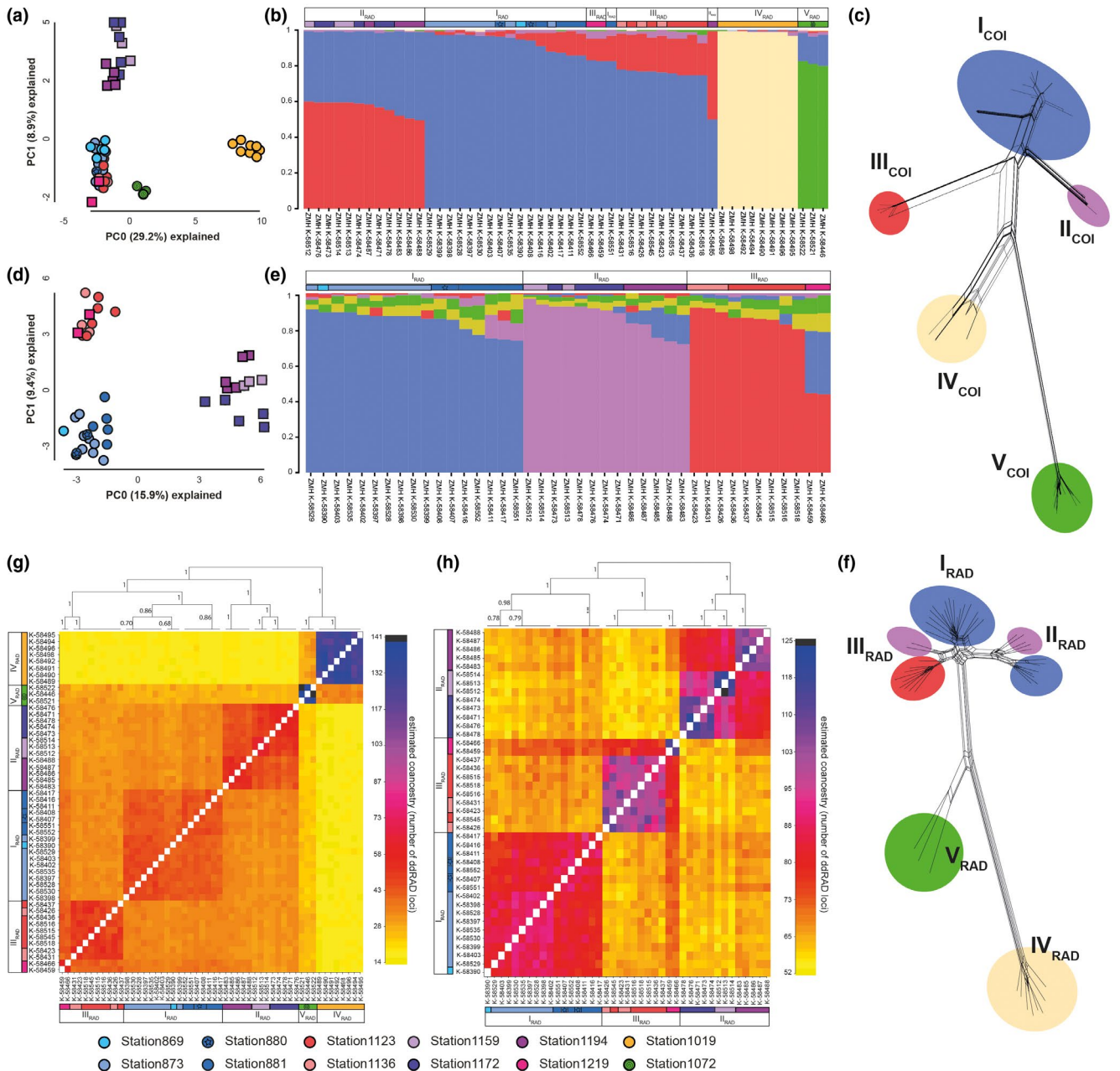


FIGURE 3 Principal component, Structure, network and coancestry analyses. (a), (d) PCA plots based on ddRAD, colours correspond to localities (Figure 1). (b), (e) Structure plots based on ddRAD showing population structure within the different lineages of *Haploniscus bicuspis*. (c) and (f) show the splittree networks calculated from COI and ddRAD, respectively. Lineages are indicated in the COI-based network and the same colour code was used in the ddRAD-based network to visualize incongruence between the two. Individuals are not shown to improve the readability of the figure (see Figure S2 for details). (g) and (h) clustered fineRADstructure coancestry matrix based on nuclear ddRAD data. Darker blue and purple colours in the matrix indicate higher proportion of loci with shared coancestry. (a), (b) and (g) include all *H. bicuspis* individuals; (d), (e) and (h) include only individuals assigned to lineages I-III. Lineages based on COI or ddRAD are indicated by the respective suffix. Colours in the legends of (b), (e), (g) and (h) correspond to localities (see Figure 1)

station 1194 into lineage II_{RAD}. The latter station had formed II_{COI} together with station 1219, however, station 1219 clustered in ddRAD with the northern stations (corresponding to III_{COI}) into III_{RAD}. As a consequence, individuals from several populations were assigned to different lineages depending on the studied markers. This was most notable at station 1219, where individuals were assigned to

II_{COI} and III_{RAD}, respectively (Figure 3a-f). However, Structure analyses assigned a relatively large fraction of ~34% of their nuclear genome to I_{RAD} (nearly as much as to III_{RAD}), but less than 3% to II_{RAD} (Figure 3b,e), suggesting limited gene flow among all three lineages. In the fineRADstructure analyses of all lineages this was not as evident, however, in the separate analyses of lineages I_{RAD}-III_{RAD},

TABLE 2 COI pairwise uncorrected p -distances in percent

	I _{COI}	II _{COI}	III _{COI}	IV _{COI}	V _{COI}
I _{COI}	0-1.77				
II _{COI}	1.61-2.64	0-0.19			
III _{COI}	2.64-3.47	3.21-3.82	0-0.38		
IV _{COI}	2.82-4.52	3.59-4.99	4.15-5.16	0-0.189	
V _{COI}	5.43-6.76	5.85-6.79	6.60-7.27	4.91-6.12	0-0.96

TABLE 3 Uncorrected p -distances of nuclear ddRAD loci in percent

	I _{RAD}	II _{RAD}	III _{RAD}	IV _{RAD}	V _{RAD}
I _{RAD}	0.08-0.17				
II _{RAD}	0.17-0.30	0.07-0.19			
III _{RAD}	0.15-0.26	0.22-0.33	0.09-0.20		
IV _{RAD}	0.72-0.89	0.77-0.91	0.71-0.89	0.11-0.16	
V _{RAD}	0.45-0.58	0.54-0.63	0.45-0.58	0.66-0.77	0.29-0.32

Note: Values are based on the analyses including all individuals.

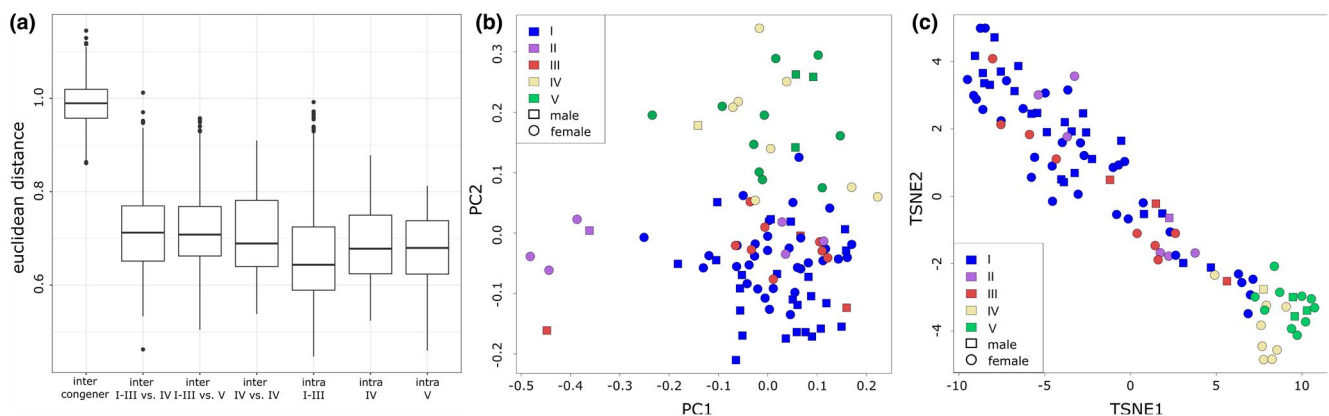


FIGURE 4 Proteomics. (a) Within and between lineage euclidean distances based on MALDI-TOF mass spectra. (b) PCA of hellinger-transformed mass spectra. (c) TSNE plot of RF model generated with three classes (I-III, IV and V). Specimens in (b) and (c) are coloured according to the respective lineages. Symbols indicate the respective sex

individuals from station 1219 exhibited the highest shared coancestry with III_{RAD} followed by I_{RAD} (Figure 3g,h). This putative hybridization might explain why I_{RAD} and III_{RAD} were not differentiated in the PCA that included all individuals, but only in the analyses focusing on lineages I-III (Figure 3a,d). South of the GIF Ridge, lineages IV_{RAD} and V_{RAD} were delimited identically to IV_{COI} and V_{COI}, respectively, without any indication of hybridization or gene flow among these two lineages or with any of the other lineages (Figure 3a-f). In the Structure analysis (Figure 3b), it appears as if V_{RAD} shared some of its genetic diversity with I_{RAD}-III_{RAD}; however, this is probably an artefact as it disappeared for larger k s and was also clearly not evident in the fineRADstructure analyses (Figure 3g).

Only two fully matured males were observed (stations 880 and 873; corresponding to lineages I_{COI} and I_{RAD}). Both featured the wider second antennular segment typical for *H. b. bicuspis*, as described by Wolff (1962). Pleopod 1 of one specimen had the two distinct corners of *H. b. bicuspis*, while the other had a more widely rounded corner, indicative of *H. b. tepidus* (Figure 2). The latter specimen thus

features a mix of characters of both subspecies. All other males were juvenile or preparatory, thus pleopod morphologies were noninformative. Their antennulae were mostly resembling *H. b. bicuspis*.

3.3 | Proteomic differentiation

In total, 96 *H. bicuspis* specimens were used in the MALDI-TOF MS analysis. Based on the COI sequences, 56 specimens were assigned to lineage I_{COI}, seven to lineage II_{COI}, 11 to lineage III_{COI}, nine to lineage IV_{COI} and 13 to lineage V_{COI}. Intraspecific Euclidean distances (pooling all lineages for *H. bicuspis*) ranged from 0.56 (10% quantile) to 0.83 (90% quantile), while intercongener distances ranged from 0.93 (10% quantile) to 1.05 (90% quantile) with very little overlap. Lineage-specific distances were all in the same range with no distinct differences, and a small tendency was found with a higher interlineage distance of I_{COI}-III_{COI} versus IV_{COI} than the intralineage distances of I_{COI}-III_{COI} (Figure 4a). The robust distance-based

multivariate analysis of variance (Wd*; Hamidi et al., 2019) revealed significant differences between lineages I_{COI} - III_{COI} , IV_{COI} , and V_{COI} ($p < .001$). The principal component analysis (Figure 4b) of the processed data shows two major groups. One comprises the specimens belonging to lineage I_{COI} - III_{COI} from the north of Iceland, and the other includes specimens of lineages IV_{COI} and V_{COI} from sampling sites south of Iceland. Based on classification votes, the TSNE plot constrained to predefined groups in a RF classification model (Figure 4c) results in a similar pattern as the PCA. In a classification approach, 98.6% of lineage I_{COI} - III_{COI} would be identified correctly with one specimen (ZMH-K 58552) being classified as lineage IV_{COI} . Similarly, one specimen of lineage IV_{COI} (ZMH-K 58494) would be classified as lineage I_{COI} - III_{COI} (11.1%), and three as lineage V_{COI} (33.3%; ZMH-K 58496, ZMH-K 58577, and ZMH-K 58579). Of lineage V_{COI} , 92.3% would be classified correctly with one specimen (ZMH-K 58521) being assigned to lineage IV_{COI} . By investigating the most important variables within the RF model based on the highest decrease in Gini Index, peaks were identified that show lineage-specific behaviour.

Lineage IV_{COI} and V_{COI} show shifts (in the range of 40–50 Daltons) in larger proteins compared to lineage I_{COI} - III_{COI} , while lineage V_{COI} and IV_{COI} were mainly separated by the relative expression of proteins with m/z of 2400, 4407 and 2680 (Figure S3). Whereas the mere presence or absence of these peaks would probably not be sufficient to distinguish between lineages, relative peak intensities differ consistently between lineages.

3.4 | Phylogeography and population genetics

In most populations, genetic diversities were not pronounced (Table S2). A few COI haplotypes are particularly common, and the majority of the other haplotypes differ by one or two mutations from one of the common haplotypes in each population and lineage (Figure 1b). Most populations feature only a few COI haplotypes. This is the case especially within lineages I_{COI} , II_{COI} and III_{COI} , as well as the populations of IV_{COI} and V_{COI} along the Reykjanes Ridge. A notable exception is population 1072 (lineage V_{COI}) to the west of Iceland, where nine haplotypes were observed. Nucleotide diversities were roughly an order of magnitude larger in the ddRAD data compared to COI (Table S2). Statistics differed slightly between the two data sets for populations and lineages in I_{RAD} , II_{RAD} , and III_{RAD} , but not extensively (Table S2). Therefore, we only focussed on the analyses of the data set which included all five lineages.

Observed heterozygosity across all ddRAD sites was close to 0.1 for all lineages and populations (Table S2). The level of inbreeding differed among lineages. Within lineages I_{RAD} - III_{RAD} and IV_{RAD} , the inbreeding coefficient F_{IS} was ≤ 0.14 for each population, but 0.18 for V_{RAD} (Table S2). Due to the Wahlund effect, F_{IS} increased (by up to 0.27) when populations were grouped into lineages I_{RAD} , II_{RAD} and III_{RAD} , or all together.

Most lineages appear to be geographically restricted and separated from each other. Lineage I_{COI} is the most widely distributed

lineage, ranging from the southeast to the northeast of Iceland around a distance of 900 km. However, the population farthest into the Nordic Seas (station 1159) is well-differentiated from the others with at least five mutations separating the observed COI haplotype from all other haplotypes (Figure 1b). Among and within all lineages, populations are strongly differentiated from each other. In the nuclear ddRAD data, population differentiation within lineages is not well resolved in the PCA and Structure analyses (Figure 3b,e), however, the coancestry analyses with fineRADstructure grouped most individuals by populations within lineages, suggesting low but detectable levels of population differentiation (Figure 3g,h). Population differentiation is particularly strong in COI, where the vast majority of populations are differentiated by significant F_{ST} values larger than 0.7, often over 0.9 (Table S3). High and significant F_{ST} values were also observed among several geographically close populations (<100 km apart), for example, station 879 compared to 880 or 881. A few instances of geographically distant but genetically similar populations in COI were observed as well: station 869 compared to 873 (210 km; lineage I_{COI}), stations 880 and 881 compared to 1172 (~450 km; lineage I_{COI}), and to a lesser degree station 83 compared to 1072 (431 km; lineage V_{COI} ; Table S3). ddRAD F_{ST} values were lower with all values within and among populations of lineages I_{RAD} - III_{RAD} being ≤ 0.29 (Table S2). Isolation-by-distance was observed in COI, though only a relatively small fraction of the genetic differentiation was explained by geographic distance (correlation coefficient $rY1 = 0.56$; $p = .001$; determination of genetic differentiation by geographic distance = 31.3%), but not in the ddRAD data (correlation coefficient $rY1 = 0.36$; $p = .15$; determination of genetic differentiation by geographic distance = 13.2%). The high levels of genetic differentiation are already observed at low geographic distances, which may explain the low correspondence between genetic differentiation and geographic distance. Furthermore, there was no correlation between F_{ST} derived from COI and F_{ST} derived from ddRAD loci (correlation coefficient $rY1 = -0.13$; $p = .164$; determination of COI F_{ST} by ddRAD $F_{ST} = 0.02\%$).

The discordance between mitochondrial and nuclear data impacts the inferred geographic distribution of genetic lineages. It is noteworthy that I_{COI} extends much farther to the northeast than I_{RAD} , whereas II_{COI} is much more restricted to the near shelf of Iceland than II_{RAD} , which extends farther to the east into the Arctic Ocean. The difference at station 1219 is the most pronounced, which has been assigned to II_{COI} , but in ddRAD appears to be a hybrid between I_{RAD} and III_{RAD} , (Figure 3c,f-h), specimens of which otherwise occur farther south or north, respectively.

Demographic parameters (Tajima's D and Fu's F_s) are slightly negative for most populations and lineages in COI, but significant only for I_{COI} (Tajima's D and Fu's F_s), III_{COI} (Tajima's D and Fu's F_s) and V_{COI} (Fu's F_s). Notable exceptions are IV_{COI} (Tajima's D and Fu's F_s significantly positive) and I_{COI} - III_{COI} jointly analysed (Fu's F_s is positive but not significant; Table S2). In the nuclear data set, most single populations had positive values close to zero (thus also lineages IV_{RAD} and V_{RAD}), however, lineages I_{RAD} , II_{RAD} , III_{RAD} and I_{RAD} - III_{RAD} each had negative values ranging from -0.13 to -0.59. The three

EBSP analyses yielded slightly diverging outcomes concerning the long-term trends. While in COI, a slightly decreasing population size over time was suggested, one of the ddRAD-based EBSPs suggested long-term stability and the other a temporal increase in population size. However, all three analyses suggest that population sizes were strongly reduced shortly before the present, followed by a rapid recovery of population sizes, probably an expansion following a bottleneck (Figure S4). It is difficult to estimate when this bottleneck may have occurred due to the lack of a conclusive specific substitution rate for isopods.

3.5 | Species distribution models

The multivariate structure test performed with the MSVF.test function on the multiclass model containing all three lineages reveals that all classes have an observed error, which is significantly lower ($p < .05$) than random error (null model, see Figure S6). This means that there is significant multivariate structure to differentiate between the three lineages using the chosen predictor variables. The multiclass model had an out-of-bag training error of 4.35%. All 161 instances of lineage I–III were correctly classified (class error = 0). Lineage IV had an error of 6.6% in which one instance out of 15 was wrongly assigned to lineage V. Lineage V had an error of 25.8%, in which eight instances out of 31 were wrongly classified as lineage IV.

The prediction of the winner class of the model is depicted in Figure 5a. Lineage I–III is distributed in the northern part of Iceland, from the shelf regions to the abyssal plains, having its southern distribution barrier along the GIF Ridge with an additional predicted occurrence south of the GIF Ridge. Lineage IV is present in the upper slope and shelf regions south of the GIF Ridge and extends into the Reykjanes Ridge at depths of around 1000 m. Lineage V extends from the abyssal plains of the North Atlantic to the north until a depth of around 1000–2000 m, and is absent in the upper slope

and shelf regions. The error rates of the presence/absence models were 0%, 6.7%, and 2.4% for lineages I–III, IV and V, respectively. The predictions for the single-lineage models are depicted in Figures S5a–c. Lineage I–III (Figure S5a) shows basically the same predicted distribution as in the multiclass model. Lineage IV, however, displays an important extension into the abyssal areas in the North Atlantic, but with low probability of 0.5–0.6 (Figure S5b). On the other hand, lineage V shows an extension into the slope areas south of Iceland up to the 500 m isobath (Figure S5c). The single-lineage models show considerable overlap in the probability of occurrence between lineages IV and V in the slope areas. In this model, lineage V is not predicted to be present along the west coast of Norway.

The niche partitioning of the lineages within the water masses is depicted in the temperature–depth plot (Figure 5b). Lineage I–III occupies the northern water mass characterized by low temperature across all depths. This lineage is mainly distributed at bottom water temperatures below 2°C. Lineage V is mainly distributed in southern water masses at temperatures between 2°C and 3°C and depths below 1000 m. Lineage IV is mainly distributed at bottom water temperatures above 3°C and depth above 3000 m, with its core distribution above 1000 m depth.

4 | DISCUSSION

4.1 | Cryptic diversity and species distributions

Delimiting species can be challenging in cases where differences between putative species are small and intraspecific variability and interspecific variation are not clearly demarcated (Hebert et al., 2003; Kaiser et al., 2021). DNA barcoding (Hebert et al., 2003) proposes a 3% threshold value, but it is obvious that delimitation is often difficult and different thresholds may exist. For example in amphipods, Radulovici et al. (2009) found intraspecific divergences

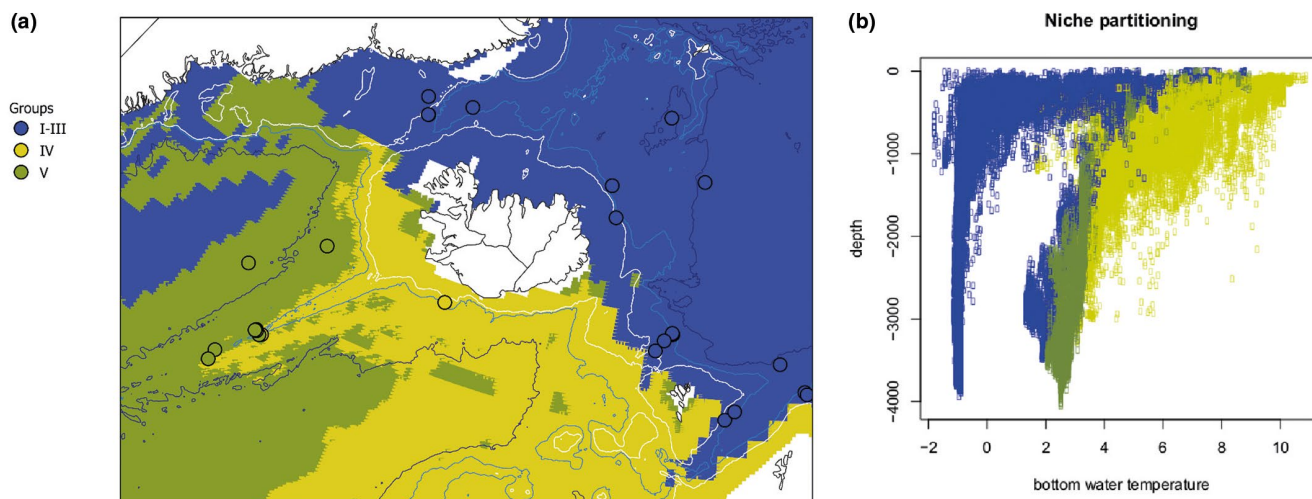


FIGURE 5 (a) Modelled distribution of the three lineages I–III, IV and V showing the respective winner class of the species distribution model; (b) temperature and depth plots showing niche partitioning for the different species

between 3.78%–13.6%, but considered the larger distances in particular as evidence for cryptic species. In the case of *Haploniscus bicuspis*, several genetically divergent lineages were recovered, of which some probably constitute separate, morphologically cryptic species. In case of the family Haploniscidae, reported distances between morphospecies in the South Atlantic Ocean ranged from 9%–20% sequence divergence (COI uncorrected p -distance, Brix et al., 2011) and from 25%–28% between genera. The high between-group divergence was contrasted by intraspecific variability lower than 1.8%. Commonly observed intraspecific COI distances within deep-sea isopods in different deep-sea isopod families were usually below 6% (e.g., Brix, Lörz, et al., 2018; Brix, Stransky, et al., 2018 for Desmosomatidae Sars, 1897; Brandt et al., 2014 for Serolidae Dana, 1852; Bober et al., 2018 for Macrostylidae Hansen, 1916), but intraspecific distances of more than 8% have been reported for example for Macrostylidae (e.g., Riehl et al., 2018). Conversely, interspecific COI distances as low as 4.6% were reported for the same family (Riehl et al., 2018), possibly suggesting that some of the larger intraspecific distances may be due to cryptic diversity, but commonly exceed 10% (e.g., in the amphipod *Eurythenes* S. I. Smith in Scudder, 1882 observed in Havermans et al., 2013; in the isopod family Serolidae in Brandt et al., 2014; as well as for desmosomatid and nannoniscid isopods in Brix, Lörz, et al., 2018; Brix, Stransky, et al., 2018). Whether the five *Haploniscus* lineages might constitute different species is discussed below.

Lineages I, II and III ($I_{\text{COI}}-III_{\text{COI}}$ and $I_{\text{RAD}}-III_{\text{RAD}}$) are consistently delimited from lineages IV and V in COI and nuclear loci, and with a few exceptions also in the proteomic data. However, these three lineages are not consistently delimited from each other. There is a clear discordance between the mitochondrial and nuclear data, with individuals being assigned to different lineages (among I, II and III) based on the respective analyses. Our data also strongly suggests multiple instances of interlineage hybridization and gene flow, which was most notable at station 1219 (see Figure 1), where gene flow between all three lineages occurred. The genetic distances in COI among these lineages are also smaller than among most other deep-sea isopods. We therefore suggest that these three lineages constitute a single species (*H. bicuspis* I–III).

Lineages IV (IV_{COI} and IV_{RAD}) and V (V_{COI} and V_{RAD}) are consistently differentiated from each other and from *H. bicuspis* I–III in COI and nuclear loci. COI p -distances between lineage V and all other lineages exceed commonly observed intraspecific distances within deep-sea isopod species. For lineage IV, COI p -distances are lower in comparison to *H. bicuspis* I–III than commonly observed among deep-sea isopods. Furthermore, the p -distances are comparable to those observed within *H. bicuspis* I–III. However, in the nuclear loci, lineage IV is the most divergent. No instances of hybridization have been inferred for lineages IV or V. Distribution modelling suggests that their habitats are ecologically differentiated from those of *H. bicuspis* I–III and are at least partially differentiated from each other. The *H. bicuspis* I–III group is distributed in the northern part of Iceland from the shelf to the deep-sea in a region influenced by the cold polar waters, while lineage IV and V are present in areas

influenced by North Atlantic waters south of Iceland as shown in Figure 5b. We therefore tentatively suggest that lineage IV and V constitute two morphologically cryptic species within *H. bicuspis* (*H. bicuspis* IV and *H. bicuspis* V, respectively).

Similar patterns of cryptic diversity have been observed for other Icelandic Isopoda, which were previously assumed to be widespread species (Brix et al., 2014; Jennings et al., 2018). The geographic distribution of the different putative *H. bicuspis* species fit well into the distribution patterns of other benthic deep-sea isopods around Iceland (Brix, Stransky, et al., 2018). Our discovery that the waters around Iceland alone may be inhabited by three cryptic species within *H. bicuspis* strongly questions the occurrence of *H. bicuspis* in the South Atlantic Ocean (Brökeland & Wägele, 2004; Menzies, 1962). The presence of further cryptic diversity in this presumably widespread species is highly likely. We deliberately did not perform molecular clock analyses to date the differentiation of the herein observed species, because evolutionary rates for deep-sea crustaceans are still lacking. A recent study suggests that the commonly applied rate of 1.4% per million years for COI (Knowlton & Weigt, 1998) is too conservative and suggested a K2P divergence of 5%–5.2% per million years for arctic marine invertebrates instead (Loeza-Quintana et al., 2019). If such rates are applicable to deep-sea benthic peracarids, such as *Haploniscus*, the divergence between the three putative species started roughly half a million to a million years ago. This is relatively young and suggests recent and putatively ongoing speciation processes.

The distribution of the three species appears to be largely governed by water masses and associated ecological parameters. In particular, the GIF Ridge represents a crucial barrier separating species. Whether the GIF Ridge is a physical barrier that hinders dispersal or just separates water masses and thereby shapes species distributions remains unanswered. The GIF Ridge has been discussed as an isolation barrier for many isopod species in the North Atlantic, for instance anthuridean isopods (Negoescu & Svavarsson, 1997), valviferan isopods (Stransky & Svavarsson, 2006), and desmosomatid and nannoniscoid isopods (Brix & Svavarsson, 2010). *Haploniscus bicuspis* sampled in this study were found between 316 m depth at station 1136 and 2422 m depth at station 1172, therefore they can easily cross the saddle depth of the GIF Ridge. Previously, *H. bicuspis* have been collected in the Arctic, even in shallow waters of 198 m depth (Brandt, 1997).

Ocean temperature is highly variable around Iceland. North of the GIF Ridge, bottom water temperature can be as low as -0.9°C , and it only becomes warmer as it reaches the shelf (up to about 3°C , Jochumsen et al., 2016). In contrast, south of the GIF Ridge, the North Atlantic water can reach up to 10.5°C (Hansen & Østerhus, 2000). Another environmental variable that may limit species distribution is the sediment structure, which was previously found to be important in peracarid crustacean distribution around Iceland (Stransky and Svavarsson, 2010). Ostmann et al. (2014) found that sediment characteristics vary in the surrounding waters of Iceland, with coarser sand found around the Reykjanes Ridge and more silt and clay found in the deep-sea east of the GIF Ridge. Oxygen

concentration may also influence migration and gene flow between isopods, especially in the deep sea. Expanding oxygen minimum zones may have contributed to allopatric speciation in the past (White, 1988; Paulus, 2021).

The distribution models provide interesting hypotheses that should be tested in future studies. These include the hypothesized distribution of *H. bicuspis* IV (and partly V), which might extend along the Norwegian coast, the occurrence of *H. bicuspis* I–III south of the GIF Ridge off the coast of Greenland, and whether *H. bicuspis* IV, V, or both occur in the abyssal plains south of Iceland. The former would require dispersal along a narrow habitable corridor along the northwest of Great Britain, whereas the expansion of *H. bicuspis* I–III south of the GIF Ridge would require crossing a region with unfavorable ecological conditions. This could have been mediated by transport via the north to south overflow of arctic deep-water. Whether *H. bicuspis* IV, V, or both occur on the abyssal plains of the North Atlantic south of Iceland cannot be answered with the available data. The ecological conditions appear suitable for both (possibly slightly better for IV), and sympatric occurrences of these two species were already observed for the Reykjanes Ridge. By examining additional populations of *H. bicuspis* genetically, future studies may shed light on these questions.

A comparison of proteomic profiles revealed differences between specimens from the northern (I–III) and southern (IV and V) species, and also between the two southern species IV and V. However, differentiation between species IV and V was less distinct. Differences between species are very small and occur mainly in a few relatively low-expressed proteins, which show differences in presence and relative intensities. Similarly, high similarity in proteomic patterns and only a small number of differentially expressed proteins were observed in cryptic mosquito species (Dieme et al., 2014; Müller et al., 2013). Like *H. bicuspis*, peaks in the mosquito *Anopheles gambiae* Giles, 1902 species complex were shifted by only a few Daltons, potentially reflecting few amino acid substitutions within proteins or minor post-transcriptional modifications (Müller et al., 2013). These small shifts in masses of specific proteins may thus infer polymorphisms of these molecules in *H. bicuspis*. Differences between the putative species were at least partly caused by a prevalence of a certain allele in the respective putative species. Despite apparent gene flow interruptions, differences between IV and V were less pronounced. Proteomic profiles depend on physiological responses to the environment, for example, variations in proteomic profiles varied with season and habitat in ticks (Karger et al., 2019). Thus, it remains unanswered whether the higher similarity of putative species IV and V results from very similar environmental impacts and thus comparable selection pressures in the past causing a similar physiological response. We interpret the high similarity between the different *H. bicuspis* species found in this study as a reflection of recent or ongoing speciation processes, as reported in fishes (Maasz et al., 2020; Takács et al., 2014). It is likely that young species are both morphologically and physiologically cryptic, revealing the limit of proteomic fingerprinting for species identification in such instances.

Haploniscus bicuspis was first described from the Norwegian Sea (Sars, 1877) north of the GIF Ridge and a few hundred kilometers east of our sampled area, but no genetic information is currently available for Norwegian representatives. Given the species' distribution around Iceland, we suggest that *H. bicuspis* I–III represents the true *Haploniscus bicuspis* (Sars, 1877), because the known and modelled distribution of *H. bicuspis* I–III extends well into the waters east of Iceland towards the Norwegian Sea and would correspond to the subspecies *H. b. bicuspis* described by Wolff (1962). However, Wolff differentiated the two subspecies based on the morphology of pleopod I, and both variants were found in *H. bicuspis* I–III (unfortunately, no adult males were available for the other two putative species). In juvenile males, the respective section of the male pleopod I is smooth and narrow and widens as they mature into preparatory males (see also Wolff, 1962). It is plausible that the different pleopod I shapes assigned to the two subspecies are in fact successive developmental stages, with the distinct corner ascribed to *H. b. bicuspis* being the later stage. Even though pleopod I morphology might not be useful to distinguish Wolff's subspecies, *H. b. tepidus* might still represent a valid species (*H. tepidus*). Whether this corresponds to *H. bicuspis* IV or *H. bicuspis* V cannot be answered with the data currently available, as *H. b. tepidus* was described from the Reykjanes Ridge.

4.2 | Phylogeography and population genetics

Historically, glacial cycles probably had a strong influence on species distributions. Most of Iceland's shelf was covered by an ice sheet during the Last Glacial Maximum (~25 ka), which broke up around 15 ka due to a northward shift of the polar front and rising sea levels (reviewed by Geirsdóttir et al., 2009). At that time, today's pattern of currents was established. The near-shelf populations of *H. bicuspis* (represented by stations 1019, 1194 and 1219) were probably colonized following the breakup of the Icelandic ice shield. Deep-sea populations farther off the coast may also have been affected by changing temperatures, currents, etc. The observed demographic history for *H. bicuspis* I–III suggests a relatively recent decline in population sizes followed by a rapid recovery, though we do not have any age estimates (Figure S4). This overall pattern might reflect population declines and local extinctions during the Last Glacial Maximum. This was then followed by population expansions and recolonizations from unaffected deep-sea regions farther off the coast during the Holocene, which were scarcely sampled in our study. Colonization from less affected regions might also explain the rapid recovery of population sizes.

Our data suggests a complex colonization history of the near-shelf regions north of the GIF Ridge for all three lineages observed within *H. bicuspis* I–III. The consistently observed differences between the mitochondrial COI and nuclear ddRAD data imply differing migration behavior between males and females. The maternally inherited COI exhibited consistently higher levels of genetic differentiation between populations, which suggests males migrate more actively and potentially over wider distances,

while females appear to be rather stationary. This is surprising, as *Haploniscus bicuspis* does not exhibit a strong sexual dimorphism in swimming structures as observed in other isopod families (e.g., Bober et al., 2018; Brix et al., 2020; Hessler, 1970; Riehl et al., 2012). However, adult males of *H. bicuspis* have stouter second antennae with many more sensory sensilla and aesthetascs than females or juvenile and preparatory males. This difference was not described by Brökeland and Wägele (2004), as they did not have adult males available in the type series. The aesthetascs are hypothesized to have a chemosensory function, possibly enabling males to detect females across large distances. This suggests that males have a more active lifestyle, roaming around in search for females, which would explain the inferred sex-specific migration patterns and the different distribution patterns of COI and ddRAD lineages. As stated in Brix et al. (2020), locomotion of the adult stages does influence migration patterns and distance for Pacific isopod families, but also a “male behaviour” is reflected in the Pacific data for Haploniscidae.

The ‘central’ region north of the GIF Ridge around stations 1194 and 1219 was probably first colonized by lineage II, possibly originating from close-by populations in the Norwegian Sea to the east or northeast of Iceland. Subsequently, males from northern (lineage III) and southern (lineage I) populations migrated into the area around station 1219, largely replacing the local population. The result is a local population at station 1219 that comprises a hybrid nuclear genome of lineages I and III, but the mitochondrial genome of lineage II. These newly arriving males must have outnumbered the local (male) population or were better adapted to the local environmental conditions, or both. We propose a similar scenario for the northeastern populations around stations 1159 and 1172. These were probably first colonized by lineage I, possibly from the central or southern Norwegian Sea, with subsequent male-biased migration and introgression from lineage II, resulting in populations with lineage I mitochondrial and lineage II nuclear genomes. The reverse, a female-biased migration and introgression, is highly unlikely in both cases due to the overall higher rates of population differentiation in COI (suggesting lower female migration rates), and because in such a scenario these females should have contributed to the nuclear genome as well.

Overall, our results show that genetic differentiation between populations is usually high, even at comparably low geographic distances, suggesting low dispersal and gene flow rates. This is also supported by elevated inbreeding coefficients in some populations, implying that reproduction occurs frequently among closely related individuals. The above-described interlineage gene flow and hybridization scenarios appear to represent rare events, which probably occurred at a time when local population densities were still low in the early phase of recolonization. The strongly male-biased migration behavior is noteworthy, with the only apparent sexual dimorphism in sensory structures. If such patterns hold true for other asellote isopods, population differentiation inferred from mitochondrial markers like COI might systematically underestimate dispersal and gene flow rates.

Haploniscus bicuspis IV is the only putative species with consistently positive values in Tajima's D and Fu's Fs, suggesting that it is currently undergoing a genetic bottleneck. At least in COI, this putative species appears closer related to *H. bicuspis* I–III, which occurs exclusively in colder arctic waters. It is possible that *H. bicuspis* IV is also better adapted to colder temperatures and is negatively affected by the northward movement of the Arctic front throughout the Holocene. The ranges of *H. bicuspis* IV and V meet along the Reykjanes Ridge, and we found *H. bicuspis* V at most stations, but with less genetic diversity among those found at the Reykjanes Ridge stations. Whether both species coexist due to the topological, structural, and environmental diversity of the Reykjanes Ridge (German et al., 1994; Taylor et al., 2021) or whether *H. bicuspis* V is currently replacing *H. bicuspis* IV is an unanswered and interesting question.

5 | CONCLUSIONS

Iceland's marine environment is comparable to a “natural laboratory” that has shaped species' distribution depending on a variety of factors. *Haploniscus bicuspis* is an Icelandic example of a benthic deep-sea species that was previously assumed to occur in all water masses around Iceland, but we have now found that there are cryptic species found within. *Haploniscus bicuspis* I–III is indicated as the “true *bicuspis*” north of Iceland. Whether species IV or V corresponds to *H. tepidus* needs to be evaluated, and they require a thorough redescription after the initial distinction by Wolff (1962).

Speciation processes in these benthic deep-sea species were probably driven by the interaction of geographic separation via the GIF Ridge with the associated ecological differences and past climatic changes. Genetic bottlenecks, potentially resulting from ice ages, were followed by population expansions into previously glaciated regions. Migration is male-biased, which results in hybrid zones and the complete exchange of the local nuclear genome in a few instances. Population genetics indicate mostly high levels of inbreeding and population differentiation, despite such cases of extensive male-biased dispersal. Such patterns may be typical for deep-sea benthic peracarid species, which are a crucial component of the fauna.

ACKNOWLEDGEMENTS

We appreciate the excellent contribution and support of the crew on the German research vessels RV Meteor, RV Poseidon, and RV Maria S. Merian. Furthermore, we are grateful to Anne-Nina Lörz (University of Hamburg) for providing support with laboratory consumables and chemicals during the research stay of EP in Hamburg. The processing of the samples would not have been possible without the technical support of Karen Jeskulke, Nicole Gatzemeier and Antje Fischer during the sorting and data management at the DZMB. Kathrin Phillipps-Bussau and Nancy Mercado Salas provided the final museum numbers from the CeNak. Thanks to Michael Sheridan for checking our English grammar. Thanks

to Jørgen Olesen and the Museum in Copenhagen for allowing access to the Wolff material of *H. b. bicuspis* and *H. b. tepidus*. Martin Kapun kindly assisted with the BayeScan analyses. Terue Kihara, Karlotta Kürzel and Alex Kienecke are thanked for making it possible to complete the CLSM pictures in Wilhelmshaven to illustrate the male developmental stages. This is publication 77 of the Senckenberg am Meer Molecular Laboratory and 13 of Proteomics Laboratory. Open access funding enabled and organized by ProjektDEAL.

AUTHOR CONTRIBUTIONS

Saskia Brix organized the expeditions and sampling. Saskia Brix and Martin Schwentner devised the project and supervised the theses of Annabelle Siebert and Eva Paulus. Species identification was performed by Saskia Brix and Jörundur Svavarsson. The COI data was generated by Annabelle Siebert and Eva Paulus, the ddRAD data by Eva Paulus, the morphological data by Annabelle Siebert and Saskia Brix; the MALDI-TOF data by Eva Paulus, Sven Rossel and Saskia Brix. The genetic data was analysed by Martin Schwentner and Eva Paulus, the MALDI-TOF data by Sven Rossel and Janna Peters. Pedro Martínez Arbizu conducted the distribution modelling. Martin Schwentner, Eva Paulus and Saskia Brix drafted the first version of the manuscript, and all authors contributed significantly to the final version.

CONFLICT OF INTEREST

The authors declare no conflicts of interest relevant to this scientific research. Funding was provided through BR3843/4-1, 5-1 and MerMet 17-06 awarded to SB from the DFG. This work was also supported by the DFG initiative 1991 "Taxon-omics" (grant no. RE2808/3-1 and RE2808/3-2).

DATA AVAILABILITY STATEMENT

All DNA sequences, were submitted to Genbank (COI: MW472427-MW472639; ddRAD in SRA: SAMN16492264-SAMN16492315; for details see Table S1). Final DNA sequence assembly was uploaded to DRYAD as well as the Random Forest input files and proteomic fingerprints findable under doi <https://doi.org/10.5061/dryad.r2280gbcd>. The BoLD data set can be found at doi [doi dx.doi.org/10.5883/DS-HAPLB](https://doi.org/10.5883/DS-HAPLB) and contains all the information about sampling locations and COI data as well as morphological identifications.

ORCID

Eva Paulus  <https://orcid.org/0000-0001-5346-2063>

Saskia Brix  <https://orcid.org/0000-0002-3269-8904>

Pedro Martínez Arbizu  <https://orcid.org/0000-0002-0891-1154>

Sven Rossel  <https://orcid.org/0000-0002-1187-346X>

Jörundur Svavarsson  <https://orcid.org/0000-0003-1842-7515>

Martin Schwentner  <https://orcid.org/0000-0002-1373-456X>

REFERENCES

Arnason, R. (2007). Climate change and fisheries: Assessing the economic impact in Iceland and Greenland. *Natural Resource Modeling*,

20(2), 163–197. <https://doi.org/10.1111/j.1939-7445.2007.tb00205.x>

- Astrin, J. J., & Stüben, P. E. (2008). Phylogeny in cryptic weevils: Molecules, morphology and new genera of Western palaeartic Cryptorhynchinae (Coleoptera: Curculionidae). *Invertebrate Systematics*, 22(5), 503. <https://doi.org/10.1071/IS07057>
- Bandelt, H. J., Forster, P., & Röhl, A. (1999). Median-joining networks for inferring intraspecific phylogenies. *Molecular Biology and Evolution*, 16(1), 37–48. <https://doi.org/10.1093/oxfordjournals.molbev.a026036>
- Bober, S., Riehl, T., Henne, S., & Brandt, A. (2018). New Macrostylidae (Isopoda) from the Northwest Pacific basin described by means of integrative taxonomy with reference to geographical barriers in the abyss. *Zoological Journal of the Linnean Society*, 182(3), 549–603. <https://doi.org/10.1093/zoolinnean/zlx042>
- Bode, M., Laakmann, S., Kaiser, P., Hagen, W., Auel, H., & Cornils, A. (2017). Unravelling diversity of deep-sea copepods using integrated morphological and molecular techniques. *Journal of Plankton Research*, 39(4), 600–617. <https://doi.org/10.1093/plankt/fbx031>
- Bouckaert, R., Vaughan, T. G., Barido-Sottani, J., Duchêne, S., Fourment, M., Gavryushkina, A., Drummond, A. J. (2019). BEAST 2.5: An advanced software platform for Bayesian evolutionary analysis. *PLoS Computational Biology*, 15(4), e1006650. <https://doi.org/10.1371/journal.pcbi.1006650>
- Boyko, C. B., Bruce, N. L., Hadfield, K. A., Merrin, K. L., Ota, Y., Poore, G. C. B., Taiti, S., Schotte, M., & Wilson, G. D. F. (2008). *World Marine, freshwater and terrestrial isopod Crustaceans database*. Accessed through: World Register of Marine Species at: <http://www.marine-species.org/isopoda> on 2020-09-04.
- Brandt, A. (1997). Biodiversity of peracarid crustaceans (Malacostraca) from the shelf down to the deep Arctic Ocean. *Biodiversity and Conservation*, 6(11), 1533–1556. <https://doi.org/10.1023/A:1018318604032>
- Brandt, A., Błażewicz-Paszkowycz, M., Bamber, R., Mühlenhardt-Siegel, U., Malyutina, M., Kaiser, S., De Broyer, C., & Havermans, C. (2012). Are there widespread peracarid species in the deep sea (Crustacea: Malacostraca)? *Polish Polar Research*, 33(2), 139–162. <https://doi.org/10.2478/v10183-012-0012-5>
- Brandt, A., Brix, S., Held, C., & Kihara, T. C. (2014). Molecular differentiation in sympatry despite morphological stasis: Deep-sea *Atlantoserolis* Wägele, 1994 and *Glabroserolis* Menzies, 1962 from the South-West Atlantic (Crustacea: Isopoda: Serolidae). *Zoological Journal of the Linnean Society*, 172(2), 318–359. <https://doi.org/10.1111/zoj.12178>
- Brandt, A., Frutos, I., Bober, S., Brix, S., Brenke, N., Guggolz, T., Heitland, N., Malyutina, M., Minzloff, U., Riehl, T., Schwabe, E., Zinkann, A.-C., & Linse, K. (2018). Composition of abyssal macrofauna along the vema fracture zone and the hadal puerto rico trench, Northern tropical Atlantic. *Deep-Sea Research Part II: Topical Studies in Oceanography*, 148, 35–44. <https://doi.org/10.1016/j.dsr2.2017.07.014>
- Breiman, L. (2001). Random forests. *Machine Learning*, 45, 5–32. <https://doi.org/10.1023/A:1010933404324>
- Brenke, N. (2005). An epibenthic sledge for operations on marine soft bottom and bedrock. *Marine Technology Society Journal*, 39(2), 10–21. <https://doi.org/10.4031/002533205787444015>
- Brix, S., Lörz, A.-N., Jazdzewska, A., Hughes, L., Tandberg, A. H., Pabis, K., Stransky, B., Krapp-Schickel, T., Sorbe, J.-C., Hendrycks, E., Vader, W. J. M., Frutos, I., Horton, T., Jazdzewski, K., Peart, R., Beermann, J., Coleman, C. O., Buhl-Mortensen, L., Corbari, L., ... Jimenez Campean, A. (2018). Amphipod family distributions around Iceland. *ZooKeys*, 731, 41–53. <https://doi.org/10.3897/zookeys.731.19854>
- Brix, S., Meißner, K., Stransky, B., Halanych, K. M., Jennings, R. M., Kocot, K. M., & Svavarsson, J. (2014). The IceAGE project - A follow up of BIOICE. *Polish Polar Research*, 35(2), 141–150. <https://doi.org/10.2478/popore-2014-0010>

- Brix, S., Osborn, K. J., Kaiser, S., Truskey, S. B., Schnurr, S. M., Brenke, N., Malyutina, M., & Martinez Arbuzo, P. (2020). Adult life strategy affects distribution patterns in abyssal isopods – implications for conservation in Pacific nodule areas. *Biogeosciences*, 17, 6163–6184. <https://doi.org/10.5194/bg-17-6163-2020>
- Brix, S., Riehl, T., & Leese, F. (2011). First genetic data for species of the genus *Haploniscus* Richardson, 1908 (Isopoda: Asellota: Haploniscidae) from neighbouring deep-sea basins in the South Atlantic. *Zootaxa*, 2838(1), 79. <https://doi.org/10.11646/zootaxa.2838.1.5>
- Brix, S., Stransky, B., Malyutina, M., Pabis, K., Svavarsson, J., & Riehl, T. (2018). Distributional patterns of isopods (Crustacea) in Icelandic and adjacent waters. *Marine Biodiversity*, 48(2), 783–811. <https://doi.org/10.1007/s12526-018-0871-z>
- Brix, S., & Svavarsson, J. (2010). Distribution and diversity of desmosomatid and nannoniscid isopods (Crustacea) on the Greenland-Iceland-Faeroe ridge. *Polar Biology*, 33, 515–530. <https://doi.org/10.1007/s00300-009-0729-8>
- Brökeland, W., & Svavarsson, J. (2017). Distribution of haploniscids (Isopoda, Asellota, Haploniscidae) in Icelandic waters, with description of *Haploniscus astraphes* n.sp. from the Iceland basin and the Southeast Atlantic Ocean. *Zootaxa*, 4231(3), 301.
- Brökeland, W., & Wägele, J. W. (2004). Redescription of three species of *Haploniscus* Richardson, 1908 (Isopoda, Asellota, Haploniscidae) from the Angola basin. *Organisms Diversity and Evolution*, 4(4), 237–239. <https://doi.org/10.1016/j.ode.2004.02.004>
- D'Alba, L., Monaghan, P., & Nager, R. G. (2010). Advances in laying date and increasing population size suggest positive responses to climate change in common eiders *Somateria mollissima* in Iceland. *IBIS*, 152, 19–28. <https://doi.org/10.1111/j.1474-919X.2009.00978.x>
- Danecek, P., Auton, A., Abecasis, G., Albers, C. A., Banks, E., DePristo, M. A., Handsaker, R. E., Lunter, G., Marth, G. T., Sherry, S. T., McVean, G., & Durbin, R. (2011). The variant call format and VCFtools. *Bioinformatics*, 27(15), 2156–2158. <https://doi.org/10.1093/bioinformatics/btr330>
- Dauvin, J. C., Alizier, S., Weppe, A., & Gudmundsson, G. (2012). Diversity and zoogeography of Icelandic deep-sea Ampeliscidae (Crustacea: Amphipoda). *Deep-Sea Research Part I: Oceanographic Research Papers*, 68, 12–23. <https://doi.org/10.1016/j.dsr.2012.04.013>
- Dieme, C., Yssouf, A., Vega-Rúa, A., Berenger, J.-M., Failloux, A.-B., Raoult, D., Parola, P., & Almeras, L. (2014). Accurate identification of Culicidae at aquatic developmental stages by MALDI-TOF MS profiling. *Parasites and Vectors*, 7(544), 1–14. <https://doi.org/10.1186/s13071-014-0544-0>
- Earl, D. A., & vonHoldt, B. M. (2012). STRUCTURE HARVESTER: A website and program for visualizing STRUCTURE output and implementing the Evanno method. *Conservation Genetics Resources*, 4(2), 359–361. <https://doi.org/10.1007/s12686-011-9548-7>
- Eaton, D. A. R., & Overcast, I. (2020). ipyrad: Interactive assembly and analysis of RADseq datasets. *Bioinformatics*, 36(8), 2592–2594. <https://doi.org/10.1093/bioinformatics/btz966>
- Edgar, R. C. (2004). MUSCLE: Multiple sequence alignment with high accuracy and high throughput. *Nucleic Acids Research*, 32(5), 1792–1797. <https://doi.org/10.1093/nar/gkh340>
- Evanno, G., Regnaut, S., & Goudet, J. (2005). Detecting the number of clusters of individuals using the software STRUCTURE: A simulation study. *Molecular Ecology*, 14(8), 2611–2620. <https://doi.org/10.1111/j.1365-294X.2005.02553.x>
- Excoffier, L., & Lischer, H. E. L. (2010). Arlequin suite ver 3.5: A new series of programs to perform population genetics analyses under linux and windows. *Molecular Ecology Resources*, 10(3), 564–567. <https://doi.org/10.1111/j.1755-0998.2010.02847.x>
- Foll, M., & Gaggiotti, O. (2008). A genome-scan method to identify selected loci appropriate for both dominant and codominant markers: A Bayesian perspective. *Genetics*, 180(2), 977–993. <https://doi.org/10.1534/genetics.108.092221>
- Franchini, P., Monné Parera, D., Kautt, A. F., & Meyer, A. (2017). quadRAD: A new high-multiplexing and PCR duplicate removal ddRAD protocol produces novel evolutionary insights in a nonradiating cichlid lineage. *Molecular Ecology*, 26(10), 2783–2795. <https://doi.org/10.1111/mec.14077>
- Geirsdóttir, Á., Miller, G. H., Axford, Y., & Ólafsdóttir, S. (2009). Holocene and latest pleistocene climate and glacier fluctuations in Iceland. *Quaternary Science Reviews*, 28(21–22), 2107–2118. <https://doi.org/10.1016/j.quascirev.2009.03.013>
- German, C. R., Briem, J., Chin, C., Danielsen, M., Holland, S., James, R., Jónsdóttir, A., Ludford, E., Moser, C., Ólafsson, J., Palmer, M. R., & Rudnicki, M. D. (1994). Hydrothermal activity on the Reykjanes ridge: The Steinahóll vent-field at 63°06'N. *Earth and Planetary Science Letters*, 121(3–4), 647–654. [https://doi.org/10.1016/0012-821X\(94\)90098-1](https://doi.org/10.1016/0012-821X(94)90098-1)
- Gibb, S. (2015). MALDIquantForeign: Import/Export routines for MALDIquant. A package for R: Retrieved from. <https://cran.r-project.org/package=MALDIquantForeign>
- Gibb, S., & Strimmer, K. (2012). Maldiquant: A versatile R package for the analysis of mass spectrometry data. *Bioinformatics*, 28(17), 2270–2271. <https://doi.org/10.1093/bioinformatics/bts447>
- Gudmundsson, G. (1998). Distributional limits of Pyrgo species at the biogeographic boundaries of the Arctic and the North-Atlantic boreal regions. *Journal of Foraminiferal Research*, 28(3), 240–256.
- Hanna, E., Jónsson, T., & Box, J. E. (2006). Recent changes in Icelandic climate. *Weather*, 61(1), 3–9. <https://doi.org/10.1256/wea.80.04>
- Hamidi, B., Wallace, K., Vasu, C., & Alekseyenko, A. V. (2019). W_d^* -test: robust distance-based multivariate analysis of variance. *Microbiome*, 7(1), 1–9.
- Hansen, B., & Østerhus, S. (2000). North Atlantic-Nordic seas exchanges. *Progress in Oceanography*, 45(2), 109–208. [https://doi.org/10.1016/S0079-6611\(99\)00052-X](https://doi.org/10.1016/S0079-6611(99)00052-X)
- Hansen, H. J. (1908). Crustacea malacostraca. In *The Danish Ingolf Expedition (1895-1896)*. 3, Copenhagen: Bianco Luno.
- Havermans, C., Sonet, G., d'Udekem d'Acoz, C., Nagy, Z. T., Martin, P., Brix, S., Riehl, T., Agrawal, S., & Held, C. (2013). Genetic and morphological divergences in the cosmopolitan deep-sea amphipod *Eurythenes gryllus* reveal a diverse abyss and a bipolar species. *PLoS One*, 8(9), e74218. <https://doi.org/10.1371/journal.pone.0074218>
- Hebert, P. D., Ratnasingham, S., & De Waard, J. R. (2003). Barcoding animal life: cytochrome c oxidase subunit 1 divergences among closely related species. (*Proceedings of the Royal Society of London Series B: Biological Sciences*, 270, (suppl_1), S96–S99.
- Hessler, R. R. (1970). *The desmosomatidae (Isopoda, Asellota) of the gay head-Bermuda transect*. University of California Press.
- Huson, D. H., & Bryant, D. (2006). Application of phylogenetic networks in evolutionary studies. *Molecular Biology and Evolution*, 23(2), 254–267. <https://doi.org/10.1093/molbev/msj030>
- Jakiel, A., Stępień, A., & Błażewicz, M. (2018). A tip of the iceberg—Pseudotanaididae (Tanaidacea) diversity in the North Atlantic. *Marine Biodiversity*, 48(2), 859–895. <https://doi.org/10.1007/s12526-018-0881-x>
- Jakobsson, M., & Rosenberg, N. A. (2007). CLUMPP: A cluster matching and permutation program for dealing with label switching and multimodality in analysis of population structure. *Bioinformatics*, 23(14), 1801–1806. <https://doi.org/10.1093/bioinformatics/btm233>
- Jennings, R. M., Brix, S., Bober, S., Svavarsson, J., & Driskell, A. (2018). More diverse than expected: Distributional patterns of Oecidiobanchus Hessler, 1970 (Isopoda, Asellota) on the Greenland-Iceland-Faeroe ridge based on molecular markers. *Marine Biodiversity*, 48(2), 845–857. <https://doi.org/10.1007/s12526-018-0857-x>
- Jennings, R. M., Golovan, O., & Brix, S. (2020). Integrative species delimitation of desmosomatid and nannoniscid isopods from the Kuril-Kamchatka trench, with description of a hadal species. *Progress in Oceanography*, 182, 102236. <https://doi.org/10.1016/j.pcean.2019.102236>

- Jochumsen, K., Schnurr, S. M., & Quadfasel, D. (2016). Bottom temperature and salinity distribution and its variability around Iceland. *Deep-Sea Research Part I: Oceanographic Research Papers*, 111, 79–90. <https://doi.org/10.1016/j.dsr.2016.02.009>
- Kaiser, S., Kihara, T. C., Brix, S., Mohrbeck, I., Janssen, A., & Jennings, R. M. (2021). Species boundaries and phylogeographic patterns in new species of *Nannoniscus* (Janiroidea: Nannoniscidae) from the equatorial Pacific nodule province inferred from mtDNA and morphology. *Zoological Journal of the Linnean Society*, 193(3), 1020–1071. <https://doi.org/10.1093/zoolinnean/zlaa174>
- Karger, A., Bettin, B., Gethmann, J. M., & Klaus, C. (2019). Whole animal matrix-assisted laser desorption/ionization time-of-flight (MALDI-TOF) mass spectrometry of ticks—Are spectra of *Ixodes ricinus* nymphs influenced by environmental, spatial, and temporal factors? *PLoS One*, 14(1), e0210590. <https://doi.org/10.1371/journal.pone.0210590>
- Knowlton, N., & Weigt, L. A. (1998). New dates and new rates for divergence across the Isthmus of Panama. *Proceedings of the Royal Society of London. Series B: Biological Sciences*, 265(1412), 2257–2263. <https://doi.org/10.1098/rspb.1998.0568>
- Kumar, S., Stecher, G., Li, M., Nknyaz, C., & Tamura, K. (2018). MEGA X: Molecular evolutionary genetics analysis across computing platforms. *Molecular Biology and Evolution*, 35(6), 1547–1549. <https://doi.org/10.1093/molbev/msy096>
- Laakmann, S., Gerdt, G., Erler, R., Kneibelsberger, T., Martínez Arbizu, P., & Raupach, M. J. (2013). Comparison of molecular species identification for North Sea calanoid copepods (Crustacea) using proteome fingerprints and DNA sequences. *Molecular Ecology Resources*, 13(5), 862–876. <https://doi.org/10.1111/1755-0998.12139>
- Legendre, P., & Gallagher, E. D. (2001). Ecologically meaningful transformations for ordination of species data. *Oecologia*, 129(2), 271–280. <https://doi.org/10.1007/s004420100716>
- Liaw, A., & Wiener, M. (2002). Classification and regression by random forest. *R News*, 2(3), 18–22.
- Lincoln, R. J. (1985). Deep-sea asellote isopods of the north-east Atlantic: The family Haploniscidae. *Journal of Natural History*, 19(4), 655–695. <https://doi.org/10.1080/00222938500770411>
- Loeza-Quintana, T., Carr, C. M., Khan, T., Bhatt, Y. A., Lyon, S. P., Hebert, P. D. N., & Adamowicz, S. J. (2019). Recalibrating the molecular clock for Arctic marine invertebrates based on DNA barcodes. *Genome*, 62(3), 200–216. <https://doi.org/10.1139/gen-2018-0107>
- Maasz, G., Zrínyi, Z., Fodor, I., Boross, N., Vitál, Z., Kánainé Sipos, D. I., Kovács, B., Melegh, S., & Takács, P. (2020). Testing the applicability of MALDI-TOF MS as an alternative stock identification method in a cryptic species complex. *Molecules*, 25(14), 3214. <https://doi.org/10.3390/molecules25143214>
- Malinsky, M., Trucchi, E., Lawson, D. J., & Falush, D. (2018). RADpainter and fineRADstructure: Population Inference from RADseq Data. *Molecular Biology and Evolution*, 35(5), 1284–1290. <https://doi.org/10.1093/molbev/msy023>
- Meißner, K., Brix, S., Halanych, K. M., & Jazdzewska, A. M. (2018). Preface—biodiversity of Icelandic waters. *Marine Biodiversity*, 48(2), 715–718. <https://doi.org/10.1007/s12526-018-0884-7>
- Meißner, K., Fiorentino, D., Schnurr, S., Martínez Arbizu, P., Huettmann, F., Holst, S., Brix, S., & Svavarsson, J. (2014). Distribution of benthic marine invertebrates at northern latitudes - An evaluation applying multi-algorithm species distribution models. *Journal of Sea Research*, 85, 241–254. <https://doi.org/10.1016/j.seares.2013.05.007>
- Menzies, R. J. (1962). The isopods of abyssal depths in the Atlantic Ocean. In J. L. Barnard, R. J. Menzies, M. J. Bacescu (Eds.), *Abyssal Crustacea*. Vema Research Series No. 1, (pp. 79–206). New York and London: Columbia University Press.
- Meyer, C. P. (2003). Molecular systematics of cowries (Gastropoda: Cypraeidae) and diversification patterns in the tropics. *Biological Journal of the Linnean Society*, 79(3), 401–459. <https://doi.org/10.1046/j.1095-8312.2003.00197.x>
- Michels, J., & Büntzow, M. (2010). Assessment of congo red as a fluorescence marker for the exoskeleton of small crustaceans and the cuticle of polychaetes. *Journal of Microscopy*, 238(2), 95–101. <https://doi.org/10.1111/j.1365-2818.2009.03360.x>
- Müller, P., Pflüger, V., Wittwer, M., Ziegler, D., Chandre, F., Simard, F., & Lengeler, C. (2013). Identification of cryptic *Anopheles* mosquito species by molecular protein profiling. *PLoS One*, 8(2), e57486. <https://doi.org/10.1371/journal.pone.0057486>
- Nachtigall, F. M., Pereira, A., Trofymchuk, O. S., & Santos, L. S. (2020). Detection of SARS-CoV-2 in nasal swabs using MALDI-MS. *Nature Biotechnology*, 38(10), 1168–1173. <https://doi.org/10.1038/s41587-020-0644-7>
- Negoescu, I., & Svavarsson, J. (1997). Anthurideans (Crustacea: Isopoda) from the North Atlantic and the Arctic Ocean. *Sarsia*, 82(3), 159–202. <https://doi.org/10.1080/00364827.1997.10413650>
- Norðdahl, H., & Ingólfsson, Ó. (2015). Collapse of the Icelandic ice sheet controlled by sea-level rise? *Arktos*, 1(13), 1–18. <https://doi.org/10.1007/s41063-015-0020-x>
- Oksanen, J., Blanchet, F. G., Kindt, R., Legendre, P., Minchin, P. R., & O'Hara, R. B. (2013). *Package vegan*. R Packag Ver 2. (vol. 2, 9th ed., pp. 1–295).
- Ostmann, A., Schnurr, S., & Martínez Arbizu, P. (2014). Marine environment around Iceland: Hydrography, sediments and first predictive models of Icelandic deep-sea sediment characteristics. *Polish Polar Research*, 35(2), 151–176. <https://doi.org/10.2478/popore-2014-0021>
- Palarea-Albaladejo, J., McLean, K., Wright, F., & Smith, D. (2018). MALDIrrpa: Quality control and robust analysis for mass spectrometry data. *Bioinformatics*, 34(3), 522–523. <https://doi.org/10.1093/bioinformatics/btx628>
- Paulus Eva (2021). Shedding Light on Deep-Sea Biodiversity—A Highly Vulnerable Habitat in the Face of Anthropogenic Change. *Frontiers in Marine Science*, 8, 1–15. <http://dx.doi.org/10.3389/fmars.2021.667048>
- Patton, H., Hubbard, A., Bradwell, T., & Schomacker, A. (2017). The configuration, sensitivity and rapid retreat of the late weichselian Icelandic ice sheet. *Earth-Science Reviews*, 166, 223–245. <https://doi.org/10.1016/j.earscirev.2017.02.001>
- Pecl, G. T., Araújo, M. B., Bell, J. D., Blanchard, J., Bonebrake, T. C., Chen, I.-C., Clark, T. D., Colwell, R. K., Danielsen, F., Evengård, B., Falconi, L., Ferrier, S., Frusher, S., Garcia, R. A., Griffis, R. B., Hobday, A. J., Janion-Scheepers, C., Jarzyna, M. A., Jennings, S., ... Williams, S. E. (2017). Biodiversity redistribution under climate change: Impacts on ecosystems and human well-being. *Science*, 355(6332), 1–9. <https://doi.org/10.1126/science.aai9214>
- Pons, J., Barraclough, T. G., Gomez-Zurita, J., Cardoso, A., Duran, D. P., Hazell, S., Kamoun, S., Sumlin, W. D., & Vogler, A. P. (2006). Sequence-based species delimitation for the DNA taxonomy of undescribed insects. *Systematic Biology*, 55(4), 595–609. <https://doi.org/10.1080/10635150600852011>
- Pritchard, J. K., Stephens, M., & Donnelly, P. (2000). Inference of population structure using multilocus genotype data. *Genetics*, 155(2), 945–959. <https://doi.org/10.1093/genetics/155.2.945>
- Peterson, B. K., Weber, J. N., Kay, E. H., Fisher, H. S., & Hoekstra, H. E. (2012). Double digest RADseq: an inexpensive method for de novo SNP discovery and genotyping in model and non-model species. *PLoS one*, 7(5), e37135.
- Puillandre, N., Lambert, A., Brouillet, S., & Achaz, G. (2012). ABGD, automatic barcode gap discovery for primary species delimitation. *Molecular Ecology*, 21(8), 1864–1877. <https://doi.org/10.1111/j.1365-294X.2011.05239.x>
- R Core Team (2020). *R: A language and environment for statistical computing*. R Foundation for Statistical Computing. <https://www.R-project.org/>
- Radulovici, A. E., Bernard, S.-M., & Dufrense, F. (2009). DNA barcoding of marine crustaceans from the estuary and Gulf of St Lawrence: A

- regional-scale approach. *Molecular Ecology Resources*, 9, 181–187. <https://doi.org/10.1111/j.1755-0998.2009.02643.x>
- Ramasamy, R. K., Ramasamy, S., Bindroo, B. B., & Naik, V. G. (2014). STRUCTURE PLOT: A program for drawing elegant STRUCTURE bar plots in user friendly interface. *SpringerPlus*, 3(431), 1–3. <https://doi.org/10.1186/2193-1801-3-431>
- Reid, N. M., & Carstens, B. C. (2012). Phylogenetic estimation error can decrease the accuracy of species delimitation: A Bayesian implementation of the general mixed Yule-coalescent model. *BMC Evolutionary Biology*, 12(1), 196. <https://doi.org/10.1186/1471-2148-12-196>
- Riccardi, N., Lucini, L., Bengali, C., Welker, M., Wicht, B., & Tonolla, M. (2012). Potential of matrix-assisted laser desorption/ionization time-of-flight mass spectrometry (MALDI TOF MS) for the identification of freshwater zooplankton: A pilot study with three *Eudiaptomus* (Copepoda: Diaptomidae) species. *Journal of Plankton Research*, 34(6), 484–492. <https://doi.org/10.1093/plankt/fbs022>
- Riehl, T., Lins, L., & Brandt, A. (2018). The effects of depth, distance, and the mid-Atlantic ridge on genetic differentiation of abyssal and hadal isopods (Macrostylidae). *Deep-Sea Research Part II: Topical Studies in Oceanography*, 148, 74–90. <https://doi.org/10.1016/j.dsr2.2017.10.005>
- Riehl, T., Wilson, G. D. F., & Hessler, R. R. (2012). New macrostylidae Hansen, 1916 (Crustacea: Isopoda) from the gay head-Bermuda transect with special consideration of sexual dimorphism. *Zootaxa*, 3277(1), 1. <https://doi.org/10.11646/zootaxa.3277.1.1>
- Rochette, N. C., Rivera-Colón, A. G., & Catchen, J. M. (2019). Stacks 2: Analytical methods for paired-end sequencing improve RADseq-based population genomics. *Molecular Ecology*, 28(21), 4737–4754. <https://doi.org/10.1111/mec.15253>
- Rossel, S., & Martínez Arbizu, P. (2018). Automatic specimen identification of harpacticoids (Crustacea: Copepoda) using random forest and MALDI-TOF mass spectra, including a post hoc test for false positive discovery. *Methods in Ecology and Evolution*, 9(6), 1421–1434. <https://doi.org/10.1111/2041-210X.13000>
- Ryan, C. G., Clayton, E., Griffin, W. L., Sie, S. H., & Cousens, D. R. (1988). SNIP, a statistics-sensitive background treatment for the quantitative analysis of PIXE spectra in geoscience applications. *Nuclear Instruments and Methods in Physics Research Section B: Beam Interactions with Materials and Atoms*, 34(3), 396–402. [https://doi.org/10.1016/0168-583X\(88\)90063-8](https://doi.org/10.1016/0168-583X(88)90063-8)
- Sars, G. O. (1877). Prodrómus descriptionis crustaceorum et pycnogonidarum, quae in expeditione norvegica anno 1876, observavit. *Mathematisk Og Naturvidenskabelig Tidsskrift*, 2, 337–368.
- Savitzky, A., & Golay, M. J. E. (1964). Smoothing and differentiation of data by simplified least squares procedures. *Analytical Chemistry*, 36(8), 1627–1639. <https://doi.org/10.1021/ac60214a047>
- Schnurr, S., Brandt, A., Brix, S., Fiorentino, D., Malyutina, M., & Svavarsson, J. (2014). Composition and distribution of selected munnopsid genera (Crustacea, Isopoda, Asellota) in Icelandic waters. *Deep-Sea Research Part I: Oceanographic Research Papers*, 84, 142–155. <https://doi.org/10.1016/j.dsr.2013.11.004>
- Schwentner, M., & Lörz, A. (2021). Population genetics of cold-water coral associated Pleustidae (Crustacea, Amphipoda) reveals cryptic diversity and recent expansion off Iceland. *Marine Ecology*, 42, e12625. <https://doi.org/10.1111/maec.12625>
- Singhal, N., Kumar, M., Kanaujia, P. K., & Virdi, J. S. (2015). MALDI-TOF mass spectrometry: An emerging technology for microbial identification and diagnosis. *Frontiers in Microbiology*, 6(791), 1–16. <https://doi.org/10.3389/fmicb.2015.00791>
- Stransky, B., & Svavarsson, J. (2006). *Astacilla boreaphilis* sp. nov. (Crustacea: Isopoda: Valvifera) from shallow and deep North Atlantic waters. *Zootaxa*, 1259(1), 1–23. <https://doi.org/10.11646/zootaxa.1259.1.1>
- Stransky, B., & Svavarsson, J. (2010). Diversity and species composition of peracarids (Crustacea: Malacostraca) on the South Greenland shelf: spatial and temporal variation. *Polar Biology*, 33(2), 125–139.
- Svavarsson, J., Strömberg, J.-O., & Brattegard, T. (1993). The deep-sea asellote (Isopoda, Crustacea) fauna of the Northern Seas: Species composition, distributional patterns and origin. *Journal of Biogeography*, 20(5), 537. <https://doi.org/10.2307/2845725>
- Takács, P., Bihari, P., Erős, T., Specziár, A., Szivák, I., Bíró, P., & Csoma, E. (2014). Genetic heterogeneity reveals on-going speciation and cryptic taxonomic diversity of stream-dwelling gudgeons (Teleostei, Cyprinidae) in the middle Danubian hydrosystem (Hungary). *PLoS One*, 9(5), e97278. <https://doi.org/10.1371/journal.pone.0097278>
- Taylor, J., Devey, C., & Brix, S. (2021). The geological and faunal composition of Steinahóll vent sites and adjacent benthos communities, Reykjanes Ridge, Iceland. *Frontiers in Marine Science*, in review.
- Taylor, M. L., & Roterman, C. N. (2017). Invertebrate population genetics across Earth's largest habitat: The deep-sea floor. *Molecular Ecology*, 26(19), 4872–4896. <https://doi.org/10.1111/mec.14237>
- Thiel, M., & Haye, P. A. (2006). The ecology of rafting in the marine environment. III. Biogeographical and evolutionary consequences. *Oceanography and Marine Biology: An Annual Review*. (vol. 44, 1st ed., pp. 323–429). CRC Press.
- Timm, L. E., Moahamed, B., Churchill, D. A., & Bracken-Grissom, H. D. (2018). Bathynomus giganteus (Isopoda: Cirolanidae) and the canyon: A population genetics assessment of De Soto Canyon as a glacial refugium for the giant deep-sea isopod. *Hydrobiologia*, 825(1), 211–225. <https://doi.org/10.1007/s10750-018-3563-6>
- Weisshappel, J. B. (2000). Distribution and diversity of the hyperbenthic amphipod family Eusiridae in the different seas around the Greenland-Iceland-Faeroe-ridge. *Sarsia*, 85(3), 227–236. <https://doi.org/10.1080/00364827.2000.10414575>
- Weisshappel, J. B. (2001). Distribution and diversity of the hyperbenthic amphipod family Calliopidae in the different seas around the Greenland-Iceland-Faeroe-ridge. *Sarsia*, 86(2), 143–151. <https://doi.org/10.1080/00364827.2001.10420469>
- White, B. N. (1988). Oceanic anoxic events and allopatric speciation in the deep sea. *Biological Oceanography*, 5(4), 243–259.
- Wilson, G. D. F., & Ah Yong, S. T. (2015). Oxygen Lifestyles of the Species-rich and Fabulous: the Deep-sea Crustaceans. *The Natural History of the Crustacea 2*. (Vol. 2, pp. 279–298).
- Wolff, T. (1962). *The systematics and biology of bathyal and abyssal isopoda asellota (Galathea Report)*. Danish Science Press.

SUPPORTING INFORMATION

Additional supporting information may be found in the online version of the article at the publisher's website.

How to cite this article: Paulus, E., Brix, S., Siebert, A., Martínez Arbizu, P., Rossel, S., Peters, J., Svavarsson, J., & Schwentner, M. (2022). Recent speciation and hybridization in Icelandic deep-sea isopods: An integrative approach using genomics and proteomics. *Molecular Ecology*, 31, 313–330. <https://doi.org/10.1111/mec.16234>